Phase Angle Dependent Ultraviolet to Far-Infrared (0.25-100 µm) Reflectance Spectroscopy of Mukundpura (CM2) Meteorite: Potential analogue of (162173) Ryugu and (101955) Bennu

I. Varatharajan[1*], A. Maturilli[1], B. Sivaraman[2], J. Helbert[1], M. Grott[1], J.K. Meka[2], S. Vijayan[2], and A. Bhardwaj[2]

[1]Institute for Planetary Research, German Aerospace Center DLR, Rutherfordstraße 2, 12489 Berlin, Germany.

[2] Physical Research Laboratory, Navrangpura, Ahmedabad, Gujarat 380009, India.

Corresponding author: Indhu Varatharajan (indhu.varatharajan@dlr.de)

Key Points:

- Band depth of diagnostic absorption features change strongly but systematically with varying viewing geometry.
- Band center of diagnostic absorption features centers are not affected by varying viewing geometry.
- Nature of 2.72 µm absorption band of Ryugu with Mukundpura fusion crust supports extensive heating in Ryugu's geologic past.

Abstract

Specialized spectral library measured under controlled planetary surface conditions is important to accurately derive the chemical and physical properties from remote observations. It's a general practice to powder the planetary analogues during spectroscopy studies as most surfaces are made up of fine-regolith materials. However, upon arrival at C-type asteroids Ryugu and Bennu, Hayabusa2 and OSIRIS-REx revealed these surfaces filled with rocks and boulders. In this study, we built a phase angle dependent ultraviolet (UV) to far-infrared (FIR) spectroscopy (0.2-100 μm) of a rocky piece of Mukundpura meteorite having five surfaces including fusion crust. Mukundpura meteorite is the freshest carbonaceous chondrite belonging to CM-chondrites in the entire collection which fell in the desert village of India on June 6, 2017. The two sets of varying viewing geometries having incident and reflectance angles includes ; a) asymmetric viewing geometry at 13°-13°, 13°-20°, 13°-30°, 13°-40°, and 13°-50°, and b) symmetric viewing geometry at 13°-13°, 20°-20°, 30°-30°, 40°-40°, and 50°-50°. This study found that overall spectral shape, reflectance values, and band depth of diagnostic absorption features are affected by viewing geometry and surface roughness; however, the fundamental band centers are not affected. The comparison of 2.72 μm absorption band of fusion crust and fresh interiors of Mukundpura with published Ryugu and Bennu spectra supports that Ryugu surface has experienced extensive heating in its geologic past compared to Bennu. Overall study shows that fusion crust and internal surfaces of the Mukundpura meteorite is a potential analogue of Ryugu and Bennu both spectrally and morphologically.

Keywords: Mukundpura, spectroscopy, C-type asteroids, phase angle, meteorite

Plain Language Summary

JAXA's Hayabusa2 and NASA's OSIRIS-REx are currently exploring two carbon-rich near-earth asteroids namely Ryugu and Bennu respectively. Different minerals characteristically absorb the received sun's energy at different wavelengths of sun's electromagnetic spectrum. Therefore, spectra recorded at wide spectral range are used as finger-prints to find the nature of minerals remote observations. However, one of the parameters that affects the spectra is viewing geometry between sun-surface-satellite. The spectrometers onboard these missions found that both asteroids possess rocky surface instead of fine-powdered soils. In this study, we spectrally investigated the non-powdered fresh carbonaceous meteorite named Mukundpura which fell in India on June, 2017 for varying viewing geometries. The sample studied has five surfaces including fusion crust. This study found that overall shape and absorption strength at characteristic wavelengths of spectra is affected by varying viewing geometry and surface roughness, however, the finger-print energy of absorption defined as band centers are not affected by these effects. The results from fusion crust and fresh meteorite surface are further compared with Ryugu and Bennu support that Ryugu surface had experienced extensive heating compared to Bennu. Overall our study shows that studied Mukundpura meteorite is a potential equivalent of Ryugu and Bennu both chemically and physically.

1 Introduction

Carbonaceous chondrites (CC) form the most important group of primitive extraterrestrial rocks that have recorded the earliest processes in the origin and evolution of solar system that includes formation of chondrules and refractory inclusions, heating records of short-lived

radionuclides, formation of planetesimals/asteroids by accretion, thermal evolution, and aqueous alteration of minerals within them [*Anders and Grevesse,* 1989]. Although CCs occupy a major fraction (75%) among asteroids, CCs only account for 4.4% including falls and finds in Earth's meteorite inventory [*Barrat et al.,* 2012]. This limits us in understanding the diversity in mineralogy and composition of C-type asteroids.

On June 6, 2017, a meteorite weighing ~2 kg fell in Mukundpura village (26° 52' 53"N, 75° 39' 54"E) of Rajasthan, India. This impact formed a nearly circular crater of ~43 cm in diameter with a depth of ~15 cm and the impactor shattered into several large pieces and numerous small pieces which weigh from gram to subgram-sized fragments [*GSI,* 2017; *Ray and Shukla,* 2018]. Mukundpura meteorite fragments were collected immediately after the reported fall and the main mass was secured by Geological Survey of India (GSI), Kolkata repository. The collected inner part of the meteorite was dark and fine to very fine grained with the development of ~1.5-2 mm thick "glossy" fusion crust containing oxidized metal and sulfides within the silicate matrix. [*GSI,* 2017] also noticed a "very strong sulfur smell" with the samples.

Ray and Shukla [2018] and *Rudraswami et al.* [2018] studied the petrography, mineralogy, isotopes, and bulk chemical composition of the samples collected and classified it as a CM2 class of carbonaceous chondrites. Therefore, Mukundpura meteorite is an extremely fresh carbonaceous chondrite in the entire CC collection. The cathode-luminescence study of the meteorite reveals [*Baliyan and Ray,* 2019] various clast and matrix-rich made of varieties of phyllosilicates, Mg-serpentine, Fe-cronstedtite, tochilinite along with; a) few relict chondrules made of highly forsteritic porphyritic olivine, barred olivine, and porphyritic pyroxene, b) isolated, subhedral olivine grains - both forsteritic ($Fo_{98.74-99.66}$) and fayalitic (Fa_{50}), c) poorly characterized phases of phyllosilicates, d) other minor and accessory phases, which includes carbonates and sulfides and e) the olivine grains within the Mukundpura meteorite suggests intense and multiple phases of complex aqueous alteration in the parent body. *Potin et al.* [2018] analysis of Mukundpura using Raman spectroscopy further confirms that Mukundpura meteorite is a primitive CM2 chondrite having escaped any significant heating including radiogenic and shock-related metamorphism.

Two sample return missions to C-type Near Earth Asteroids (NEAs), JAXA's Hayabusa2 mission to (162173) Ryugu (1999 JU3) and NASA's Origins, Spectral Investigation, Resource Identification, Security-Regolith Explorer (OSIRIS-REx) mission to (101955) Bennu, carry spectrometers of varying spectral ranges for remote sensing mapping.

Hayabusa2 carries two onboard remote sensing spectrometers; The Telescopic Optical Navigation Camera (ONC-T) with seven color filters (ul: 0.40 µm, b: 0.48 µm, v: 0.55 µm, Na: 0.59 µm, w: 0.70 µm, x: 0.86 µm, and p: 0.95 µm) [*Tatsumi et al.,* 2019] and the Near-Infrared Spectrometer (NIRS3) operating in scanning mode and collecting reflectance spectra in the range from 1.8 – 3.2 µm with spectral sampling resolution of 18 nm.

OSIRIS-REx carries two spectrometers; OSIRIS-REx Visible and Infrared Spectrometer (OVIRS) which covers the spectral range of 0.4–4.3 µm with a 4-mrad field of view (FOV) and a spectral sampling of 2 nm from 0.392 to 2.4 µm, and 5 nm from 2.4 to 4.3 µm [*Reuter et al.,* 2018; *Simon et al.,* 2018], and OSIRIS-REx Thermal Emission Spectrometer (OTES), which covers the spectral range 5.5–100 µm with an 8-mrad FOV and a spectral sampling of 8.66 cm^{-1} [*Christensen et al.,* 2018]; both aiming to map the spatially resolved global composition at 20 m and 40 m respectively.

Hayabusa2 and OSIRIS-REx shows that both Ryugu and Bennu are very dark top-shaped body (visible albedo of 4.6% with photometry standard reflectance lower than 2% [*Sugita et al.,*

2019] for Ryugu) with a very rocky surface covered by numerous boulders (10 cm to 10 m sized boulders for Ryugu) with almost no regolith [*DellaGiustina et al.,* 2019; *Lauretta et al.,* 2019; *Sugita et al.,* 2019; *Walsh et al.,* 2019; *Watanabe et al.,* 2019]. For a correct interpretation of the remote sensing spectral data it is therefore important to understand the spectral behaviour of CCs having varying 3-dimentional (3D) surface roughness (not just powders) belonging to this particular asteroid class (C-type) at wide spectral range from ultraviolet (UV: 0.25 μm) to far-infrared (FIR: 100 μm) and varying phase angle combinations.

Beck et al. [2018], *Jacinto et al*. [2013], and *Malavergne et al.* [2014] studied the laboratory spectroscopy of various powdered carbonaceous chondrites of varying grain sizes under vacuum conditions to characterise their corresponding asteroid parent bodies. However, the dependency of the reflectance spectra on their varying observation geometry and phase angles for its corresponding spectral regions is still largely unknown for these chondrites [*Beck et al.,* 2018]. In a recent study, *Potin et al.* [2019] studied the varying spectral nature of the Mukundpura chip and powder corresponding to varying viewing geometries and temperatures but limiting to VNIR spectral region (0.34 - 5 μm) in order to characterise the NEAs and found that the spectral slopes, reflectance values, and absorption bands are affected by these effects.

In this study, we carried out reflectance spectroscopy of the fresh Mukundpura CM2 meteorite rock (non-powdered) at wide spectral range (UV:0.2- FIR:100 μm) under varying viewing geometries with phase angles varies from 26° to 100° respectively (Fig. 1). In addition to understanding the mineralogy of the Mukundpura (CM chondrite) from a spectroscopy standpoint, we also investigated the overall spectral behaviour (UV-FIR) of Mukundpura meteorite for its overall spectral shape, slope, absorption band centres, and band strength as a function of viewing geometry and surface roughness. Therefore, this study will help to carefully interpret the remote sensing and landing site spectra of the rocky surfaces of Ryugu, Bennu, and future missions exploring NEAs.

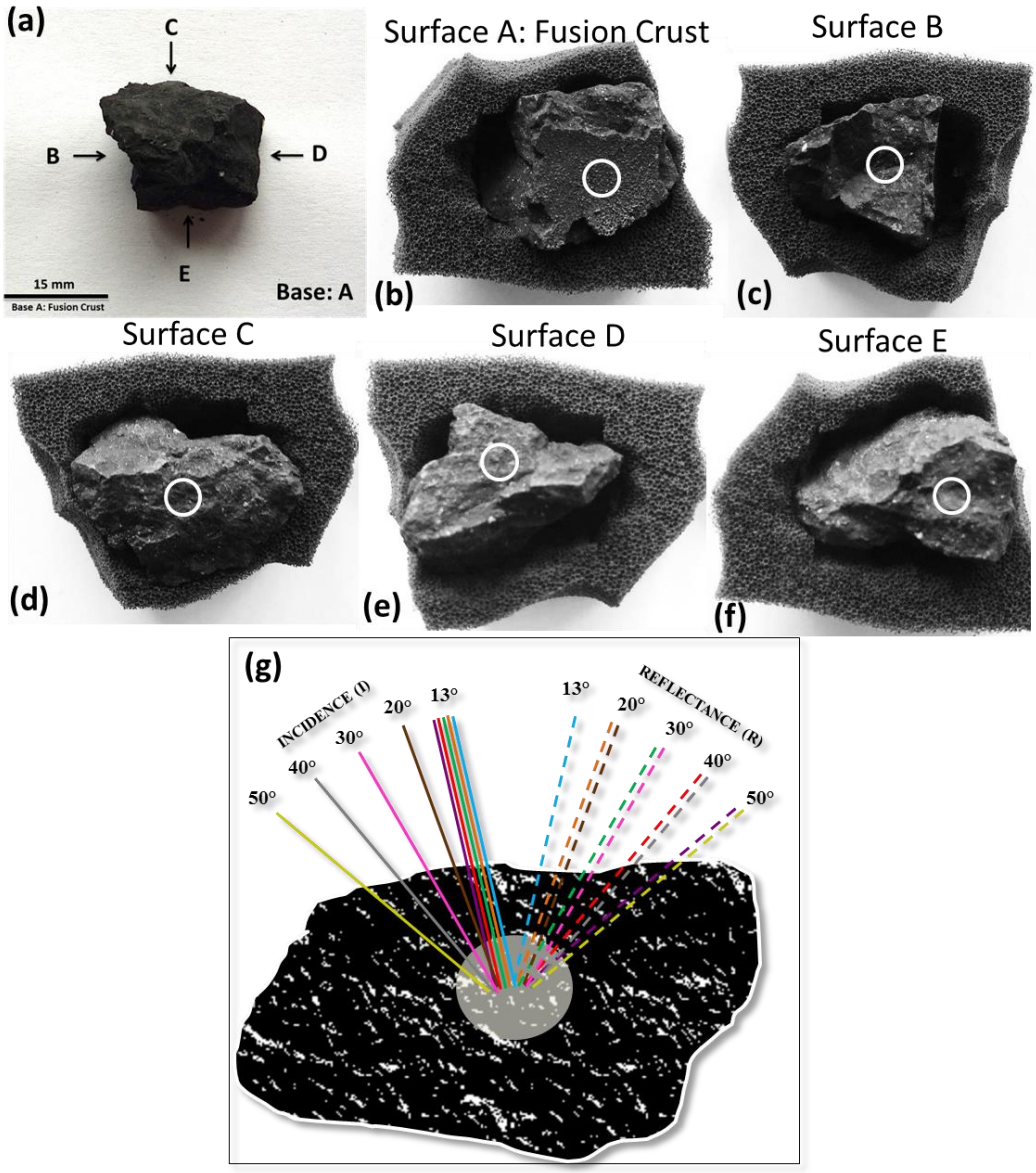

Figure 1. a) the scale of Mukundpura meteorite studied sitting on its fusion crust, b-f) different surfaces (surfaces B-E) of Mukundpura sample where the white circle represents the (approx) area of region studied for spectral analyses. The brightness and contrast of the picture is enhanced to clear representation of roughness of the surface – resembling asteroid Ryugu, g) the symmetric (13°-13°, 20°-20°, 30°-30°, 40°-40°, 50°-50) and asymmetric (13°-13°, 13°-20°, 13°-30°, 13°-40°,13°-50°) viewing geometries with varying phase angles considered in this study.

2 Sample

In this study we used a small sample from the fresh Mukundpura meteorite (CM chondrite) (Fig. 1) without powdering it. This provides a better morphological analog since the sample closely resembles the rocky surface of Ryugu and Bennu. The sample collected (Fig. 1a)

has five different surfaces/sides including the fusion crust (Fig. 1b; surface A) and four interior surfaces (Fig. 1c-f; surfaces B-E). During the impact parts of Mukundpura broke into small fragments and the sample collected and studied in this manuscript has a surface exhibiting fusion crust (surface A) and the fresh interior surfaces (surfaces B-E). By measuring the mass (5.7841 gm) and computing the volume (2.5426 cm^3), we then calculated the bulk density (=mass/volume) of the Mukundpura sample and found to be 2.2749 g/cm^3 typical for CM chondrites [*Flynn et al.,* 2018]. The computation of volume of the sample is enabled by 3D mapping of the sample using NextEngine3D scanner and its corresponding 3D shape (.stl format) is provided as supporting information.

The bright spots on the surface of the rock in Fig.1a indicate the presence of CAIs. The fusion crust (Fig. 1b; surface A) is nearly flat and glossy surface, which is a very thin layer formed due to melting of the outer surface as the meteorite falls through the atmosphere. Fig. 1b-f shows the surfaces of the Mukundpura meteorite studied, which is placed on the sponge sample holder in-order to fix them steadily while taking the measurements. The white circle placed on each surface in Fig. 1b-f indicates the approximate area studied in the spectral analyses for the respective spectral region for varying viewing geometry. The brightness and contrast of Fig. 1b-f is enhanced to emphasize the differences in the 3D surface roughness/topography of each of the surfaces resembling the rocky/boulder-rich surface on the asteroids Ryugu and Bennu.

3 Methods

In this study, the phase angle dependent bi-conical reflectance spectroscopy of the Mukundpura sample is carried out at the Planetary Spectroscopy Laboratory (PSL) facility located at the Institute of Planetary Research (PF) at the German Aerospace Center (DLR), Berlin [*Maturilli et al.,* 2018b]. Two Bruker Vertex 80V instruments hosted at PSL are used for the reflectance measurements (Fig. 2a); one of the spectrometers (Bruker A; Fig. 2a) is equipped with aluminum mirrors and therefore optimized for spectral measurements in the ultraviolet (UV: 0.2-0.6 μm), visible-infrared (VISIR: 0.4-1 μm) range, mid infrared (MIR: 1-25 μm), and the second one (Bruker B; Fig. 2) is equipped with gold-coated mirrors optimized for measurements in Far infrared (FIR: 14-100 μm).

Both the spectrometers (Bruker A and Bruker B) use a Bruker A513 variable-angle reflection accessory (Fig. 2b) attached with two mirrors enabling viewing cone with aperture of 17° and therefore allowing bi-conical reflectance measurements under vacuum conditions for varying viewing geometry with phase angles between 26° and 170° [*Beck et al.,* 2018; *Maturilli et al.,* 2018a; *Maturilli et al.,* 2014].

The UV-FIR spectroscopy of each surface of the Mukundpura sample is conducted for two sets of varying viewing geometries for a total of nine phase angle combinations (Fig. 1g); a) asymmetric viewing geometry where incident angle is fixed near nadir (13º) and reflectance angles varied in steps: 13°-13°, 13°-20°, 13°-30°, 13°-40°, and 13°-50°, and b) symmetric viewing geometry, where both incidence and reflectance angles varied identically with respect to each other for each measurement which includes 13°-13°, 20°-20°, 30°-30°, 40°-40°, and 50°-50°. In order to achieve this, we obtained a total of 225 spectra (5 surfaces times 9 phase angle combinations times 5 sets of detector-beamsplitter configurations to cover the entire spectral range).

We collected bi-conical reflectance spectra under vacuum for five meteorite surfaces (A-E; Fig. 2) in the whole spectral range (~0.2–100 μm) using both spectrometers. The details of the beam-splitter and detector used for each spectral subset are tabulated in Table S1 in supporting

information. The reflectance of each Mukundpura surface was measured at a spectral resolution of ~4cm^{-1} using a spot size of 4 mm at nine different phase angle combinations. The references used for calibration in each spectral range are also listed in Table S1. The measured reflectance spectrum of each surface at each phase angle is then divided by the corresponding reflectance spectrum of the reference at the respective phase angle. For details on the step-by-step procedure of the reflectance measurements, see Text S1 of the supporting information. The average surface spectra (throughout the manuscript) is calculated by taking the mean of the spectra at their respective viewing geometry for the surfaces B, C, D, and E.

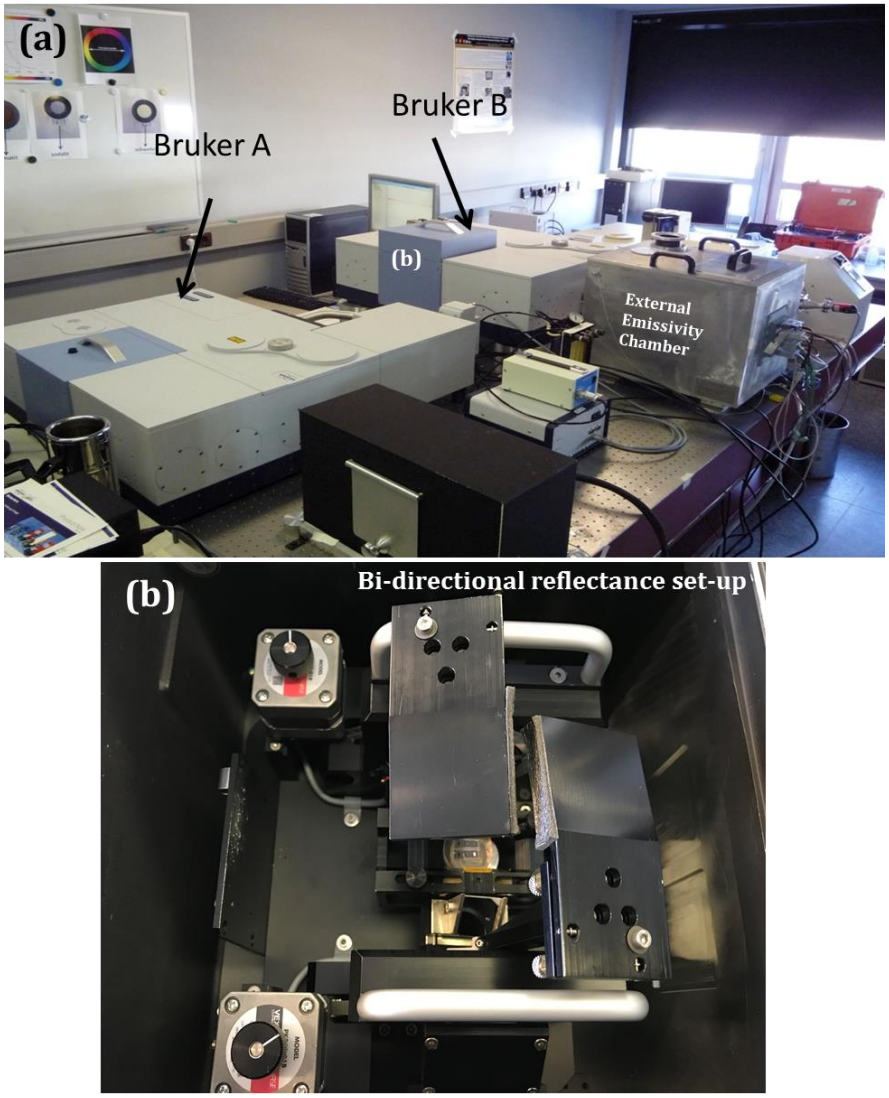

Figure 2. a) Laboratory set-up at PSL. Both Bruker A and Bruker B are Bruker Vertex 80V FTIR spectrometers. Bruker A is optimized for measurements in UV, VIS-IR, TIR spectral range and Bruker B is optimized for measurements in FIR spectral range. Bruker B is also attached to an external emissivity chamber for direct emissivity measurements at very high temperatures. b) shows the bi-conical reflectance setup at PSL.

3.1 Derivation of spectral parameters

3.1.1 Continuum-Removal

We have derived commonly used spectral parameters, such as band center and the band depth of diagnostic absorption features, to understand their behaviour with changing phase angle combinations and local surface roughness (e.g., Section 4.3). In order to achieve this, the reflectance spectra are first normalized with respect to a common baseline by adopting the continuum removal methodology by *Clark et al.* [1987] and *Clark and Roush* [1984]. This is achieved by first fitting the convex-hull over the absorption feature by anchoring the continuum shoulder points having maximum reflectance values on either side of the absorption feature. Continuum removed spectra are then derived by diving the reflectance spectra with this continuum baseline.

3.1.2 Band Center and Band Depth

The band center is the wavelength of the band minima of a diagnostic absorption feature (where maximum absorption occurs) in the continuum removed spectra. Band depth is estimated as 1-continuum removed reflectance value at the calculated band minima i.e., band center.

4 Results

The UV-FIR spectra of Mukundpura sample for two sets of viewing geometries are shown in Fig. 3. The spectra of at phase angle combinations 13°-30° (green), 13°-40° (red), and 13°-50° (violet), behaves relatively different with enhanced spectral features at longer wavelengths (> 9 μm) irrespective of the surfaces compared to other viewing angles.

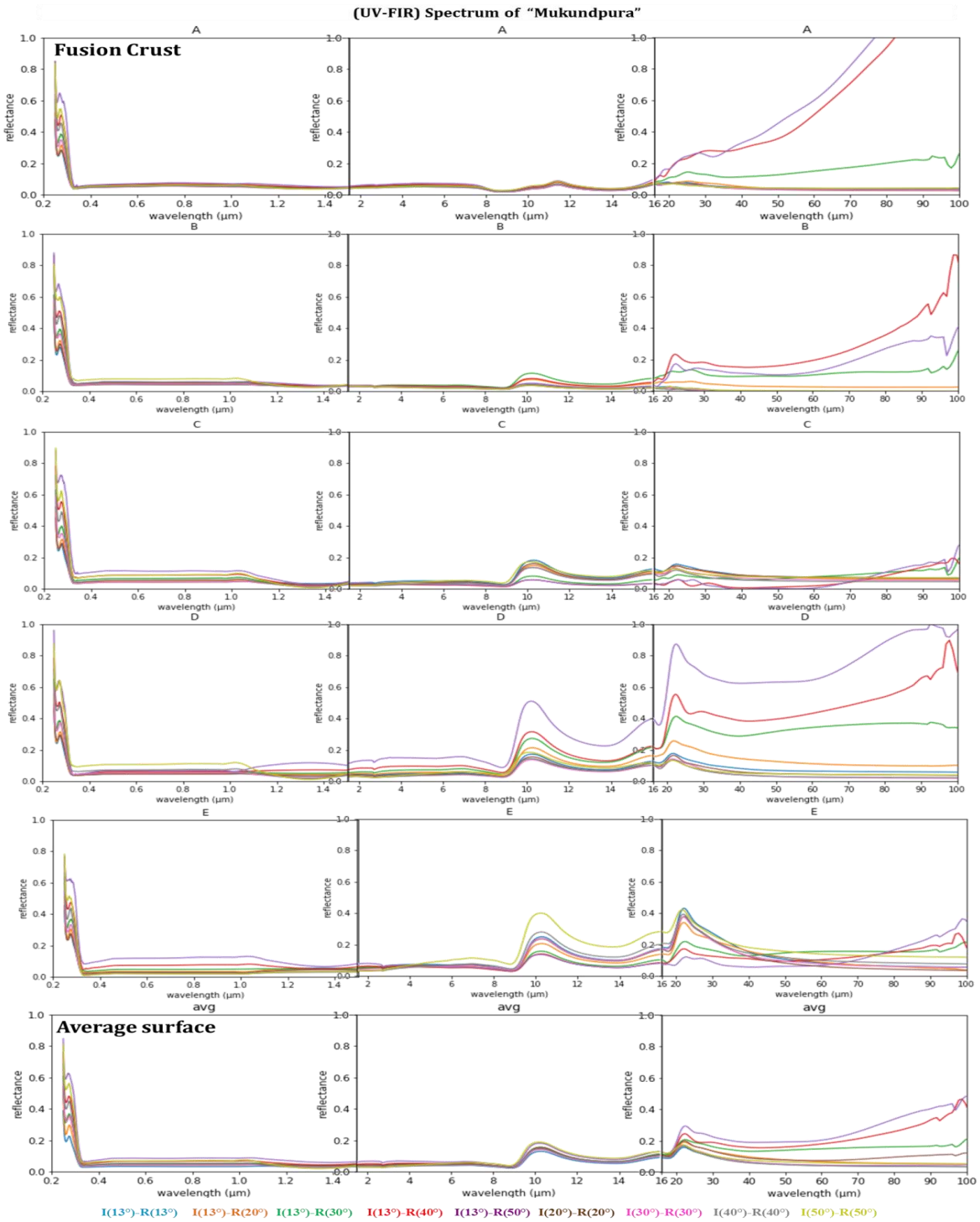

Figure 3. Measured UV-FIR spectra of fusion crust (A), intrinsic surfaces (B-E), and the average spectra of surafces (B-E) for its varying viewing geometry

4.1 Ultraviolet (UV): 0.2-0.6 μm

In the UV-VIS region, both fusion crust (Fig. 4A) and the other meteorite surfaces (Fig. 4B-E) show spectral characteristics; with strongest reflectance near 0.25 μm, a narrow

absorption feature near ~0.26 μm with reflectance peak at 0.275 μm, a steeper bluer (negative) slope from 0.27 to 0.325 μm, and a very low reflectance with nearly flat spectra from 0.325 to 0.6 μm. *Applin et al.* [2018] analysis on the UV reflectance spectra of carbonaceous materials reveals that all varieties of pure carbon revealed a Fresnel peak (sp^2 π–π^*) short-ward of 0.3 μm and the position of this peak maximum changes with grain size and metamorphism and spectral contrast of Fresnel peak decreases with grain size where smaller grain sizes peaks near 0.272 μm and the larger macroscopic grained powders of amorphous carbon peaks near 0.25 – 0.26 μm. Therefore, the Fresnel peaks near 0.25 μm and 0.275 μm of fusion crust and surface spectra of Mukundpura suggests the presence of nanophase graphite or amorphous carbon in the matrix [*Applin et al.,* 2018].

For all the five sides of the meteorite (Fig. 4 A-E), the reflectance value at Fresnel peak near 0.275μm and thereby the spectral slope between 0.275-0.325 μm increases with increasing reflectance angle irrespective of their incidence angle. For all the five surfaces, longward of 0.325 μm the spectral variation diminishes, and no distinguishable signature is present at any viewing geometry. This suggests that, irrespective of the surface roughness, the UV-VIS spectral nature of Mukundpura sample have similar behavior at their respective phase angle observations. Altogether, it corresponds to the presence of carbon rich matrix within all surfaces including fusion crust [*Applin et al.,* 2018]. The dark carbonaceous material in visible region is highly reflective in the UV region (0.25-0.3 μm).

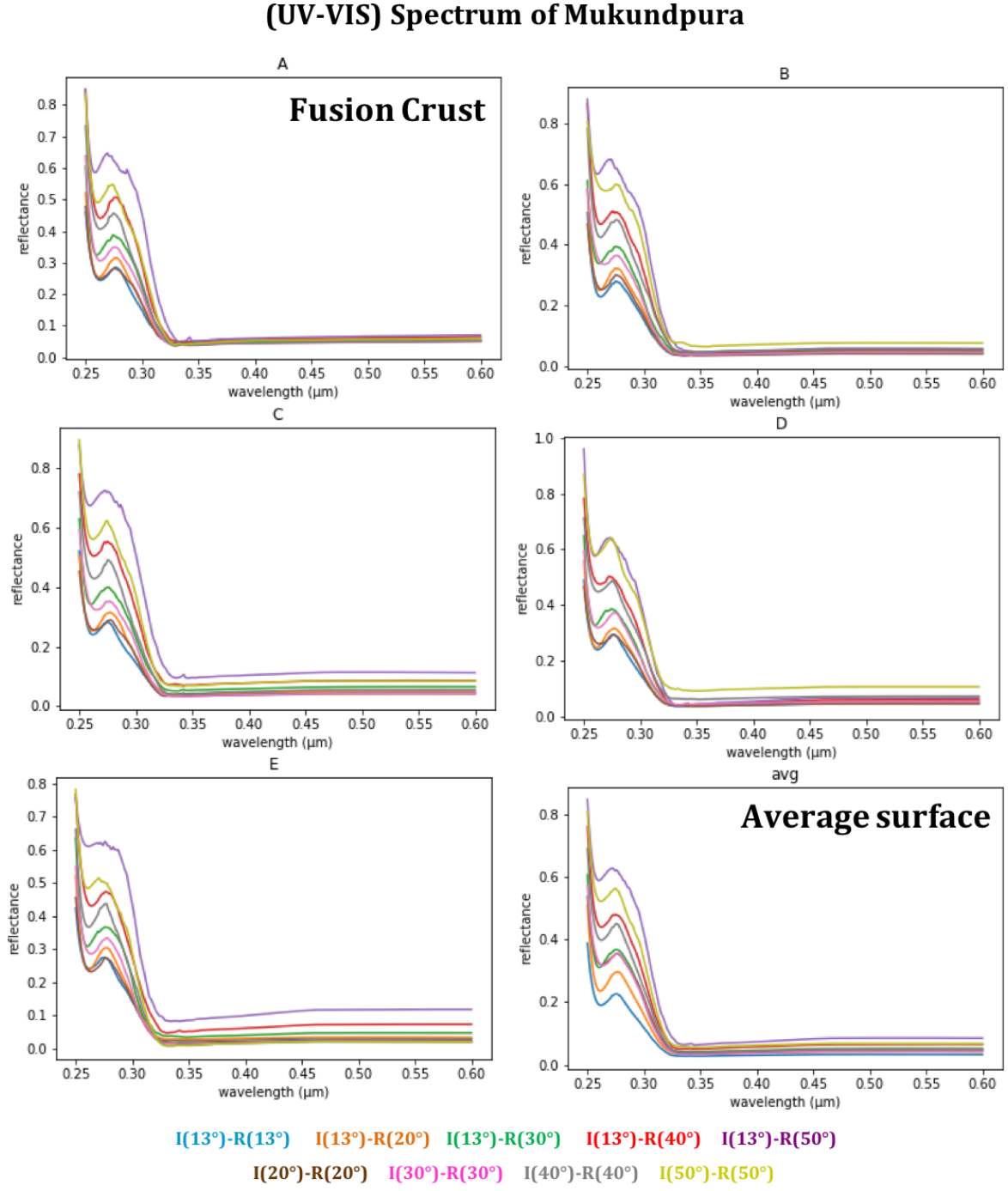

Figure 4. UV spectra of fusion crust (A), intrinsic surfaces (B-E), and the average spectra of surafces (B-E) for its varying viewing geometry

4.2 Visible – Infrared (VIS-IR): 0.4-1 μm

Fig. 5i shows the absolute VIS-IR reflectance of all surfaces including fusion crust (A) and average spectra (Avg) of all internal meteorite surfaces (B-E). Fig. 5ii shows the normalized VIS-IR reflectance spectra of Mukundpura obtained normalizing the spectra at 0.55 μm for its corresponding phase angle the same normalization method used for spectral analysis of ONC-T

data [*Tatsumi et al.,* 2019]. The normalized spectra in Fig. 5ii are also resampled to the Hayabusa 2 ONC-T spectral bands (ul: 0.40 µm, b: 0.48 µm, v: 0.55 µm, Na: 0.59 µm, w: 0.70 µm, x: 0.86 µm, and p: 0.95 µm) [*Tatsumi et al.,* 2019] for the corresponding surfaces and phase angles. Fig. 5iii is the color/visible slope plot between v-to-p slope ($Ref_{0.55}/R_{0.95}$) and ul-to-v slope ($Ref_{0.40}/Ref_{0.55}$) which helps to understand the visible color variations for different Mukundpura surfaces including the fusion crust and the different viewing geometries for each surface.

The VIS-IR spectra of CM chondrites are generally characterized by modestly blue- to red slopes and usually show a characteristic absorption band around ~0.7 µm associated with a ~0.9-1.1 µm absorption band [*Beck et al.,* 2018; *Cloutis et al.,* 2011]. *Cloutis et al.* [2011] studied the VIS-IR spectral properties of 39 CM chondrites at viewing angles i = 30º and e = 0º and found that in general overall slope of VIS-IR spectra range from blue-sloped to red-sloped with brighter spectra being more red-sloped and matrix-enriched CM spectra are more blue-sloped than bulk samples. The ~0.7 µm absorption feature is associated with Fe^{2+} and Fe^{3+} charge transfer and the 0.9 µm absorption band is attributed to Fe^{2+} crystal field transitions in Fe-bearing phyllosilicates within the CMs [*Cloutis et al.,* 2011]. The 0.7 µm absorption band is also correlated with the amount of water and therefore related to the presence and abundance of phyllosilicates in the CMs studied [*Beck et al.,* 2018]. Also, there are correlation between reflectance value at 0.55 µm and the carbon content in the CMs [*Beck et al.,* 2018; *Cloutis et al.,* 2011].

Fusion crust (Surface A; Fig. 5): All VIS-IR spectra of fusion crust have weak broad convex spectral shape with the reflectance maximum centered on 0.7 µm and the reflectance of 0.05 for the overall spectral range (Fig. 5i A); except for phase angle 50º-50º (Fig. 5i A: olive). Normalizing the fusion crust spectrum (Fig. 5ii A) enhances the convex shape for all phase angles showing the spectra is blue-sloped to red-sloped with the spectral inflection at 0.7 µm; in other words, the absence of the characteristic 0.7 µm absorption band, suggesting the loss of water in the serpentines/phyllosilicates [*Beck et al.,* 2018] due to the atmospheric heating during the meteorite fall. The color slope plot for the fusion crust (Fig. 5iii A) shows that there are no considerable variations within the ul-to-v slope (blue slope) where the values are roughly concentrated around 0.3 suggesting that ul-to-v slope is not affected by varying viewing geometry for the fusion crust. However, v-to-p slope (red slope) in the slope plot (Fig. 5iii A) exhibits a slight linear behavior where the slope increases roughly with increase in phase angle/viewing geometry with the highest value of 0.05 (+ve) for phase angle 50º-50º (Fig. 5iii A; olive) and least value of -0.12 for phase angle 13º-13º (Fig. 5iii A; blue). It is important to note that, all v-to-p slope have negative values except for the value at phase angle 50º-50º (Fig. 5iii A; olive). However, all spectra have a downturn behavior after 0.85 µm which may correspond to contributions from Fe-bearing minerals such as Fe-poor phyllosilicates, Fe-cronstedtite, and/or Fe-olivine within the matrix/chondrules [*Cloutis et al.,* 2011].

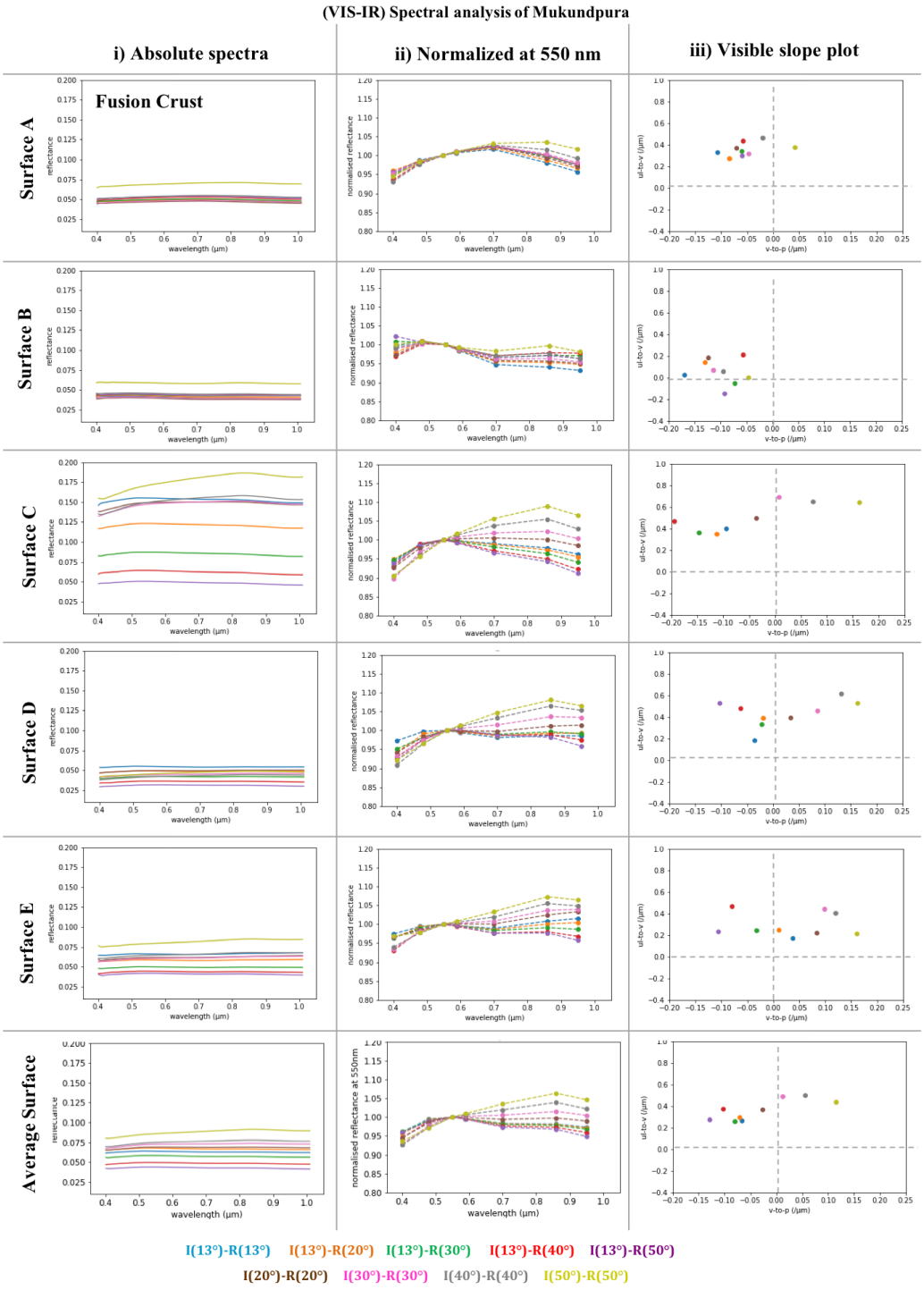

Figure 5. i) Absolute VIS-IR spectra, ii) Normalized spectra at 0.55 μm, iii) spectral parameter plot between v-to-p slope ($Ref_{0.55}/R_{0.95}$) and ul-to-v slope ($Ref_{0.40}/Ref_{0.55}$) for fusion crust (A), intrinsic surfaces (B-E), and the average spectra of surafces (B-E) for its varying viewing geometry.

4.2.1 Absolute VIS-IR spectra of Internal Mukundpura surfaces

The absolute reflectance spectra of fresh Mukundpura surfaces (Fig. 5i B-E) shows that reflectance behavior of surface B (Fig. 5i B) for varying viewing geometry for the corresponding phase angles show only small variations except for phase angle 50º-50º (olive).

The reflectance spectra of surface C (Fig. 5i C) shows most variations among the phase angles compared to rest of the surfaces B-E. The overall reflectance of the spectra obtained for asymmetric viewing geometry and increasing phase angles have significantly linear behavior; 13º-13º (blue) > 13º-20º (orange) > 13º-30º (green) > 13º-40º (red) > 13º-50º (violet). However, the symmetric viewing geometry with increasing phase angle (13º-13º, 20º-20º, 30º-30º, 40º-40º, and 50º-50º) have only small differences in the reflectance values for the overall spectra. The spectra show an increase in reflectance with different geometry and the highest reflectance is obtained for phase angle 50°-50° with diagnostic change in slope (Fig. 5i C; olive). However, the red-sloped spectral region until 0.8 µm increases slightly with increasing phase angles.

VIS-IR reflectance for surfaces D (Fig. 5i D) and E (Fig. 5i E) have very similar behavior with nearly flat spectral shape and narrow linear variations in the reflectance values among the different viewing geometry. The reflectance spectra at phase angle 50º-50º for surface E however has the brightest spectrum and slightly stronger red-slope (Fig. 5i E; olive).

4.2.2 Spectral Dependency on Phase Angle and Surface roughness

Among normalized VIS-IR spectra for all surfaces (Fig. 5ii B-E), surface B shows different spectral behavior than rest of the surfaces for all phase angles including the fusion crust (Fig. 5ii B). Also, there is no particular trend between corresponding v-to-p slope and ul-to-v slope for the normalized spectra of surface B (Fig. 5iii B). This behavior could be explained by either surface B being matrix enriched compared to the other surfaces which would correspond to bulk samples [*Cloutis et al.,* 2011], or it could be simply due to the intrinsic surface roughness. For all phase angle observations, the v-to-p slope have negative values (red slope), but the ul-to-p slope values spread from negative (red slope) to positive (blue slope) values, which is also evident from the normalized surface B spectra in Fig. 5ii B). Importantly, spectra of surface B for all phase angles have a weak absorption feature near 0.7 µm (attributable to Fe^{2+}-Fe^{3+} charge transfer) and a IR downturn after 0.88 µm (ascribable to Fe^{2+} d-d crystal field transitions); both of these features suggests the presence of Fe-poor serpentines in the matrix [*Cloutis et al.,* 2011]. These absorption features are also observed in the powdered sample of Mukundpura meteorite in the study by *Izawa et al.* [2019].

After normalization, the surfaces C-E shows very similar spectral shape for the corresponding phase angle of each surface C, D, and E (Fig. 5ii C, D, E) irrespective of the differences in the surface roughness among the surfaces. The spectral slope ul-to-v is positive (blue-sloped) for all phase angles of all the three surfaces C, D, and E (Fig. 5ii C, D, E). On the other hand, the v-to-p spectral slope shows a strong linear trend with the corresponding phase angle observation for all the three surfaces C, D, E (Fig. 5ii C, D, E) whose values changes from positive (red sloped) to negative (blue-sloped) in the order of decreasing phase angles for symmetric viewing geometry and increasing phase angles for asymmetric viewing geometry; 50º-50º > 40º-40º > 30º-30º > 20º-20º > 13º-13º > 13º-20º > 13º-30º > 13º-40º > 13º-50º. It is also interesting to note that in general cases v-to-p slope for symmetric viewing geometries (50º-50º > 40º-40º > 30º-30º > 20º-20º > 13º-13º) have positive values (blue-sloped) and v-to-p slope for the asymmetric viewing geometries (13º-13º > 13º-20º > 13º-30º > 13º-40º > 13º-50º) have negative

values (red-sloped). All the spectra show IR downturn after 0.88 µm which may correspond to Fe-bearing minerals [*Cloutis et al.,* 2011]. On the other hand, the 0.7 µm absorption is not evident for all phase angles observations for surface C; however, a minor feature could be traced for surfaces D and E for phase angles say 13º-40º (Fig. 5ii D, E; red) and 13º-50º (Fig. 5ii D, E; violet). Unlike surface B which has both 0.7 and 0.9 µm absorption feature suggesting a matrix-enriched surface and/or with Fe-bearing hydrous minerals, the behavior of evident IR downturn after 0.88 µm with weak or no 0.7 µm absorption features for surfaces C, D, E may correspond to the surface containing bulk representation of matrix and chondrules containing crystalline anhydrous minerals (possibly Fe-bearing olivine within the chondrules) along with Fe-poor serpentines within the matrix [*Cloutis et al.,* 2011].

4.3 Near Infrared (NIR): 1 – 5 µm

NIR spectroscopy is sensitive to the presence OH and H_2O groups within the rocks and allows inferring the mineralogy of hydrated/hydrous carbonaceous chondrites [*Beck et al.,* 2010; *Farmer,* 1974; *Hamilton et al.,* 2019; *Hiroi et al.,* 1996; *Matsuoka et al.,* 2019]. One of the characteristic spectral parameter of CM chondrites in the NIR spectral region is the presence of diagnostic sharp asymmetric absorption feature near the 3 µm water/OH absorption band. The strength of the band is due to the combination of stretching ν_1 and anti-stretching ν_3 vibration modes of water (H_2O) [*Beck et al.,* 2010].The position of band minima (band center at maximum absorption) at 3 µm feature is attributed to the stretching vibrations of the hydroxyl groups in the octahedral layer of phyllosilicates probing the local cationic environment (tetrahedral cations) [*Ryskin,* 1974]; the band minima at 2.72 µm corresponds to Mg-OH and the band minima at 2.82 µm corresponds to Fe-OH [*Beck et al.,* 2018; *Beck et al.,* 2010; *Cloutis et al.,* 2011; *Hiroi et al.,* 1996; *McAdam et al.,* 2015; *Takir et al.,* 2013]. The 3 µm band is usually accompanied by the second narrow reflectance minimum around 2.95 µm. The shape of this 3 µm is attributed to the chemistry of the phyllosilicates and mineralogy of the samples [*Beck et al.,* 2010; *Browning et al.,* 1996; *Howard et al.,* 2009; *Takir et al.,* 2013]. Weaker absorption features around 3.4-3.5 µm and sometimes at 2.3 µm is attributed to Mg-OH in serpentines and C-H stretching from organics [*Beck et al.,* 2018]. The presence of a reflectance minimum around 3.1 µm is commonly attributed to adsorbed water [*Beck et al.,* 2010].

Absolute NIR spectra of all the surfaces including the fusion crust of Mukundpura sample studied (Fig. 6i) show nearly feature-less spectra overall except with the prominent 3 µm absorption feature. In order to better understand the relation of phase angle observations and surface roughness on the band shape and band center, we take a closer look at the following spectral parameters; a) normalized spectra where the reflectance at 2 µm is normalized to one (Fig. 6ii); to better understand the minor slope changes with respect to phase angle and surface roughness, b) continuum removed spectra with continuum shoulders at 1.5 and 4 µm to derive the spectral parameters of diagnostic absorption feature at 3 µm, c) the band center vs band depth; to quantitatively understand the nature of 3 µm spectral feature (Fig. 6iv), their corresponding clay mineralogy, and their spectral dependency on phase angle of observation and surface roughness.

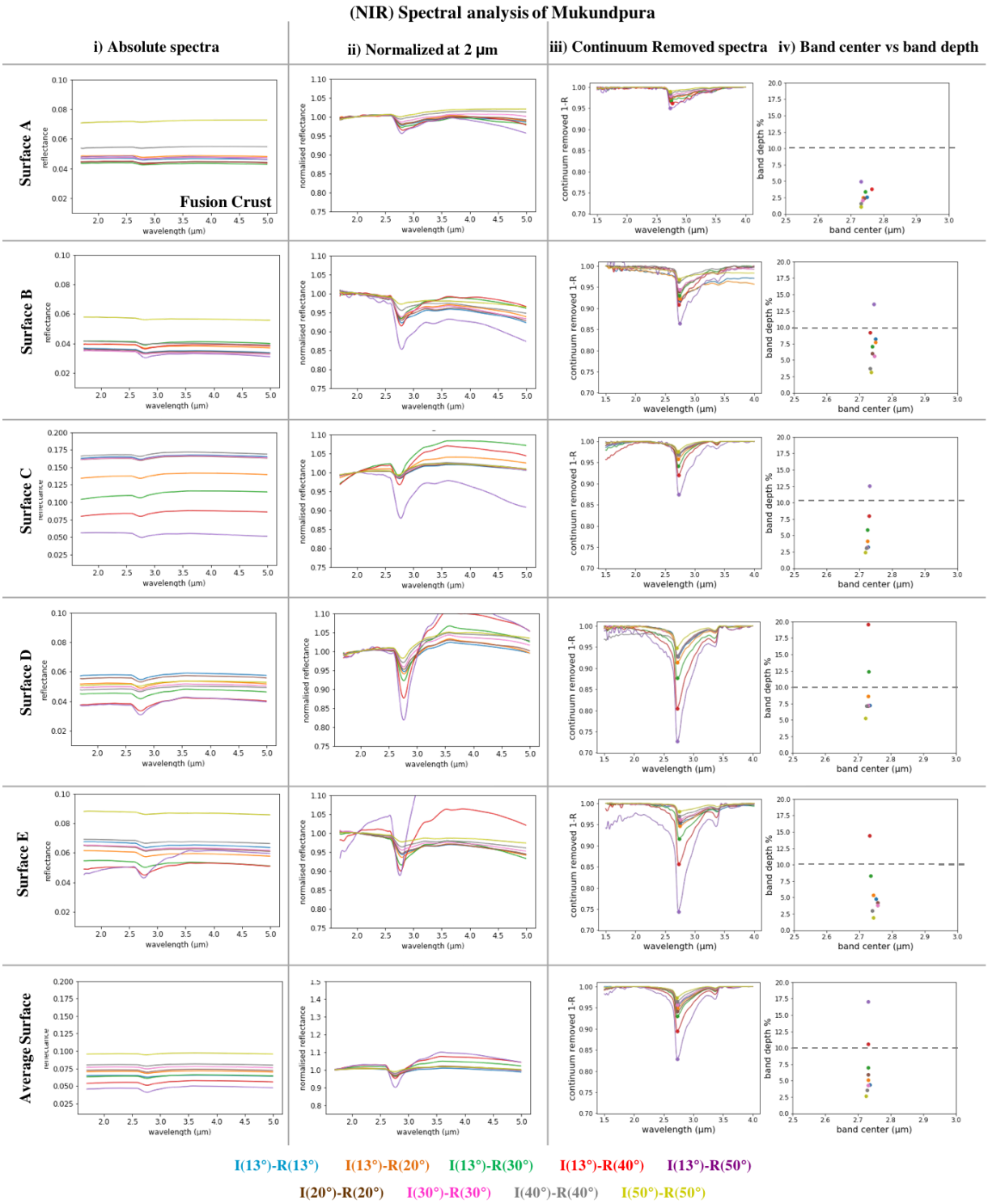

Figure 6. i) Absolute NIR spectra, ii) Normalized spectra at 2.0µm, iii) continuum removed spectra between 1.5 and 4 µm , iv) spectral parameter plot between 3 µm band center and absorption band depth for fusion crust (A), intrinsic surfaces (B-E), and the average spectra of surafces (B-E) for its varying viewing geometry.

Fusion crust (Fig. 6ii-iv A): The normalized NIR spectra of the fusion crust (Fig. 6ii A) show that the strength of the 3 µm is highly subdued and varies with phase angle of observation. The normalized spectra (Fig. 6ii A) for phase angle 50º-50º is nearly flat (Fig. 6ii A; olive) with weak absorption near 3 µm, whereas the phase angles 13º-40º (Fig. 6ii A; red) and 13º-50º (Fig. 6ii A; violet) have stronger 3 µm along with weak absorption features around 3.4 µm confirming the presence of Mg-serpentines and C-H stretching [*Beck et al.,* 2018] of organics and also have a negative spectral slope after 4 µm. The continuum removed spectra (Fig. 6iii A) shows the highly asymmetrical 3 µm absorption band and the band-center vs band-depth plot (Fig. 6iii A) shows that the band center of the 3 µm features centers around 2.72-2.75 µm with < 2% absorption for most phase angles with the exception of 2-5% absorption for phase angles 13º-30º (Fig. 6iv A; green), 13º-40º (Fig. 6iv A; red) and 13º-50º (Fig. 6iv A; violet). The weak 3 µm absorption feature of fusion crust is attributed to the loss of water (OH) due to the atmospheric heating during entry; and the 2.72 µm is attributed to the loss of water within the Mg-serpentine.

Mukundpura surface (Fig. 6ii-iv B-E): The normalized NIR spectra (Fig. 6iii B-E) shows that the spectral slope and shape is highly dependent on the phase angle and the surface topography. The normalized NIR spectra of surface B (Fig. 6iii B) at all phase angles have a slight negative slope at all NIR wavelengths; however, the remaining surfaces (Fig. 6iii C-E) have positive slope upto 3.5 µm and a negative slope afterwards (3.5-5 µm). Such differences are not obvious in the not normalized spectra (Fig. 6ii B-E). Among the phase angle of observations for all surfaces, the normalized spectra for phase angles 13º-40º (Fig. 6ii B-E; red) and 13º-50º (Fig. 6ii B-E; violet) show the strongest spectral shape and features such as spectral slopes and absorption strength. Spectra for phase angles 50º-50º (Fig. 6iv B-E; olive) have the least contrast in spectral shape and features. The continuum removed spectra (Fig. 6iii B-E) and the band center vs band depth at 3 µm plot (Fig. 6iii B-E) of all fresh Mukundpura surfaces for all phase angles and surface roughness displays evident narrow asymmetric absorption feature with a band center around 2.72 µm. It remains almost constant irrespective of varying surface roughness and phase angles (Fig. 6iii-iv B-E) and this band position corresponds to the Mg-OH stretching modes observed in Mg-phyllosilicates [*Beck et al.,* 2010; *Takir et al.,* 2013]. However, the strength of these absorption features varies with respect to phase angle of observation whose values are generally less than 10% (Fig. 6iv B-E) except for phase angles 13º-40º (Fig. 6iv B-E; red) and 13º-50º (Fig. 6iv B-E; violet) which have strongest absorptions in some cases up to 27% (Fig. 6iii D; violet). On careful examination, the minor spectral inflection showing the evidence of a weak 2.95 µm absorption accompanying the strongest ~2.72 µm absorption feature is evident for the continuum removed NIR spectra at phase angles 13º-40º (Fig. 6iii B-E; red) and 13º-50º (Fig. 6iii B-E; violet). The continuum removed spectra for all surfaces (Fig. 6iii B-E) also displays a weaker but evident ~3.4 µm absorption feature for all phase angles with the strongest features for 13º-40º (Fig. 6iii B-E; red) and 13º-50º (Fig. 6iii B-E; violet), further confirming the presence of Mg-serpentines in the Mukundpura sample studied. The absence of any ~3.1 µm band for all NIR spectra of surfaces and fusion crust confirms that there is no adsorbed water [*Beck et al.,* 2010] in the meteorite surfaces and the measurements are taken in vacuum conditions.

The NIR region shows that the band absorption strength for 2.72 µm is highly dependent on the phase angle of observation and surface flatness/roughness. This must be carefully taken into consideration while performing quantitative analysis such as correlating the shape and strength of the 3 µm absorption band to characterize the level of hydration [*Beck et al.,* 2014;

Garenne et al., 2016; *Garenne et al.,* 2014] when analyzing the remote sensing/landed surface spectral data of carbonaceous asteroids as Ryugu and Bennu.

4.4 Mid Infrared (MIR): 5-16 µm

The spectral band shape and position in the MIR region is widely studied for the evidence of the presence and nature of phyllosilicates, their hydrous alteration state, and therefore gives information on the initial composition of anhydrous minerals in the meteorite [*Howard et al.,* 2009, 2011; *Tomeoka and Buseck,* 1985]. When the primitive meteorites alter, the first Fe-matrix of the anhydrous silicates convert to phyllosilicates and then the Mg-rich silicates within the chondrules starts to alter as the process progresses [*McAdam et al.,* 2015]. The late stage of alteration therefore tends to produce predominantly Mg-rich serpentines [*McAdam et al.,* 2015]. The phyllosilicate alteration phases of CM chondrites are mostly composed of various serpentines [*Barber,* 1981; *Glotch et al.,* 2007; *Hanowski and Brearley,* 2001; *Lauretta et al.,* 2000; *MacKinnon,* 1982; *Richardson,* 1981; *Zega and Buseck,* 2003; *Zolensky et al.,* 1993].

Reflectance spectra of surfaces A-E (Fig. 7i; A-E): The MIR spectrum (5-16 µm) of all surfaces of Mukundpura sample possess three characteristic spectral features; a) sharp Christiansen Feature (CF) minimum centered near ~9 µm, b) reflectance maximum centered near 10.5 µm, and c) broad absorption feature extending from 10-16 µm with the center around 14 µm. However, the strength and the nature of these bands vary with respect to the surface roughness and the phase angle combinations. The stronger spectral shape for all different surfaces is observed in the spectra taken at phase angle of 13º-40º (Fig. 7i C-E; red) and 13º-50º (Fig. 7i C-E; violet) whereas the weakest spectral shape is attributed to the observations made at phase angle 50º-50º (Fig. 7i C-E; olive).

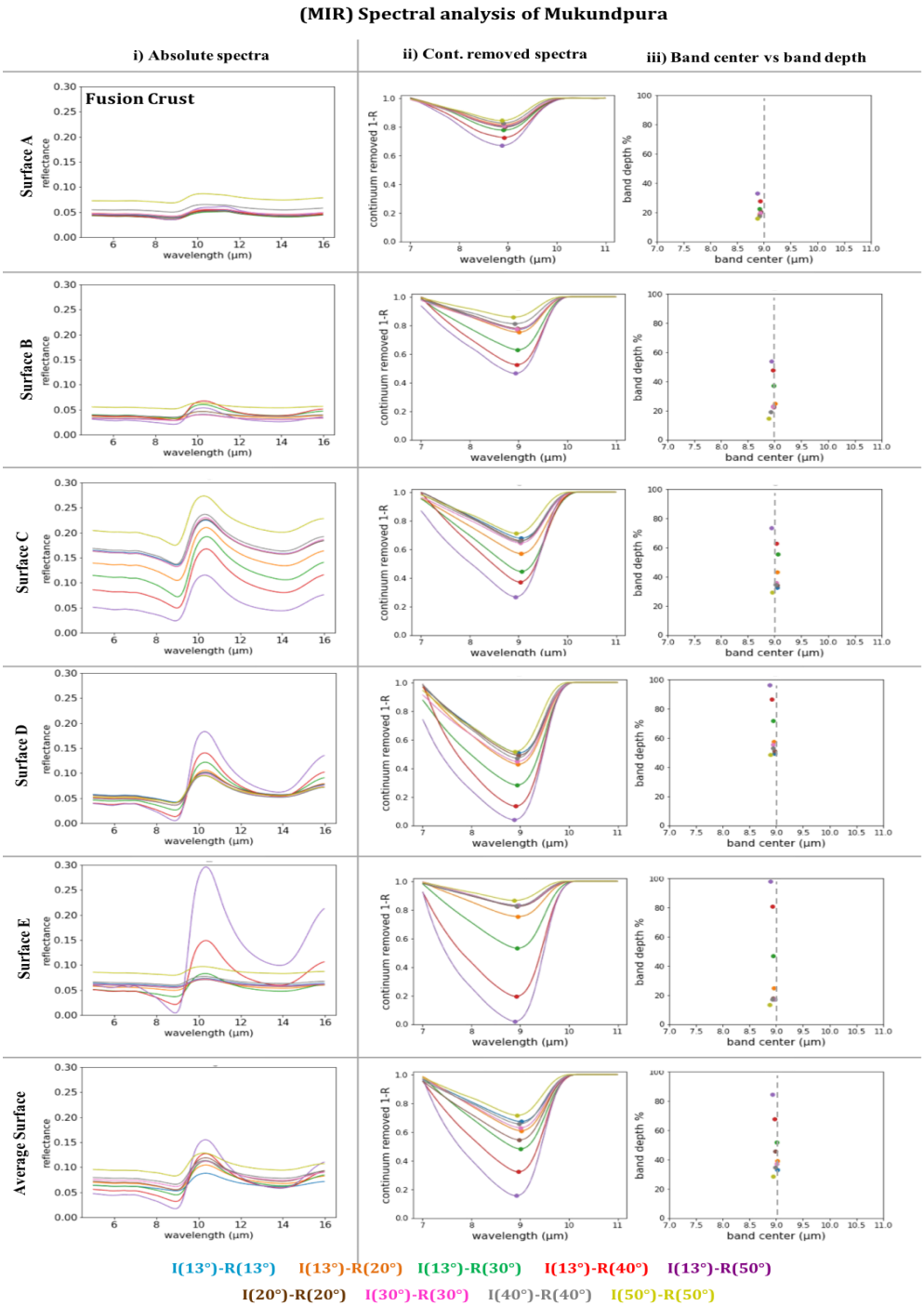

Figure 7. i) Absolute MIR spectra, ii) continuum removed spectra between 7 and 11 μm , iii) spectral parameter plot between 9μm band center and absorption band depth for fusion crust (A), intrinsic surfaces (B-E), and the average spectra of surafces (B-E) for its varying viewing geometry.

The spectral shape of the Mukundpura sample and their characteristic spectral features, CF minimum at 9 μm and the reflectance maximum at ~10.5 μm, are attributed to the stretching modes of SiO_4 bonds in serpentine, specifically resembling Mg-serpentine sample, Burminco

from Mariposa County, CA, USA (BUR-1690; $(Mg_{2.81}Fe_{0.35})(Si_{1.87}Al_{0.07})O_5(OH)_4$) in the spectroscopy study by *Glotch et al.* [2007] and therefore spectrally confirming the presence of dominant Mg-serpentines in the matrix of Mukundpura, which is also suggested in the study by *Haberle et al.* [2019].

In order to study the dependency of Christiansen feature minimum (~9 μm) for its spectral parameters such as band center vs band depth (Fig. 7iii;A-E) in relation to observations at varying phase angle and surface roughness, we first performed continuum removal of the spectra by fitting the convex-hull over the 9 μm absorption feature by anchoring the continuum end points at reflectance values at 7 and 11 μm (See Section 3.1.1 for methods) as shown in Fig.7ii; A-E, average spectra). For all the surfaces including the fusion crust, the continuum removed spectra of all meteorite surfaces (Fig. 7ii; A-E) for the phase angle combinations 13º-30º (Fig. 7A-E; green), 13º-40º (Fig. 7A-E; red) and 13º-50º (Fig. 7A-E; violet) shows strongest band absorption whereas 50º-50º (Fig. 7A-E; olive) shows the weakest absorption at 9 μm.

The band center versus band depth values plotted at Fig. 7iii (A-E) are calculated by finding the band minima and the band depth at ~9 μm in the corresponding continuum spectra (See Section 3.1.2 for methods). Fig. 7iii (A-E) shows that irrespective of the phase angle of observation and the surface roughness, the band center for all the surfaces (Fig. 7iii B-E) including the thermally altered fusion crust (Fig. 7iii A) is unchanged and centered at ~9 μm. Therefore, the band center value at 9 μm spectral parameter acts as a stable spectral parameter that could be used to trace the presence of serpentines across the remote sensing targets. On the other hand, the absorption band depth at 9 μm is affected by thermal alteration (fusion crust; Fig.7iii-A) and viewing angles (Fig.7iii; A-E). It is important to note that, for any surface the band depths have extreme (high) values for phase angles at 13º-30º (Fig. 7i B-E; green), 13º-40º (Fig. 7i B-E; red) and 13º-50º (Fig. 7i B-E; violet); however, for other phase angles the band depths don't have significant variations. This is important because at extreme viewing angle remote sensing observations of asteroid targets such as Ryugu (Hayabusa2) and Bennu (OSIRIS-REx), the band depth of the spectra should be carefully used for quantitative interpretation such as abundance of phyllosilicates/serpentines [*Maturilli et al.*, 2016; *Potin et al.*, 2019]. This behavior is also seen in the thermally altered fusion crust (Fig, 7iii A); however, the band depths are subdued for all phase angles due to loss OH in the structure of serpentines.

Except for the MIR spectra of fusion crust (Fig. 7i;A), all the surface spectra (Fig. 7i; B-E, Avg) shows a minor broad absorption feature near 6 μm feature which is pronouncedly present in the phase angles 13º-40º (Fig. 7i B-E; red) and 13º-50º (Fig. 7i B-E; violet), which is also evidently visible in the average surface spectra (Fig. 7i; Avg). This 6 μm absorption feature is attributed to presence of bending modes of water molecules, specifically interlayer water of the clay minerals [*Beck et al.*, 2010; *Garenne et al.*, 2014], Mg-serpentine in the case of Mukundpura.

4.5 Far Infrared (FIR): 16-100 μm

The FIR region of Mukundpura sample shows very complex spectral behavior with respect to roughness and phase angle of measurement. The measurements at phase angles13º-40º (Fig. 8B-E; red) and 13º-50º (Fig. 8B-E; violet) shows a very broad absorption feature extending 22-90 μm, and the strength of this absorption varies with surface roughness eg., surface Fig.8 (C, D, E). This absorption feature is not evident in remaining phase angle observations with the nearly flat and dark spectra.

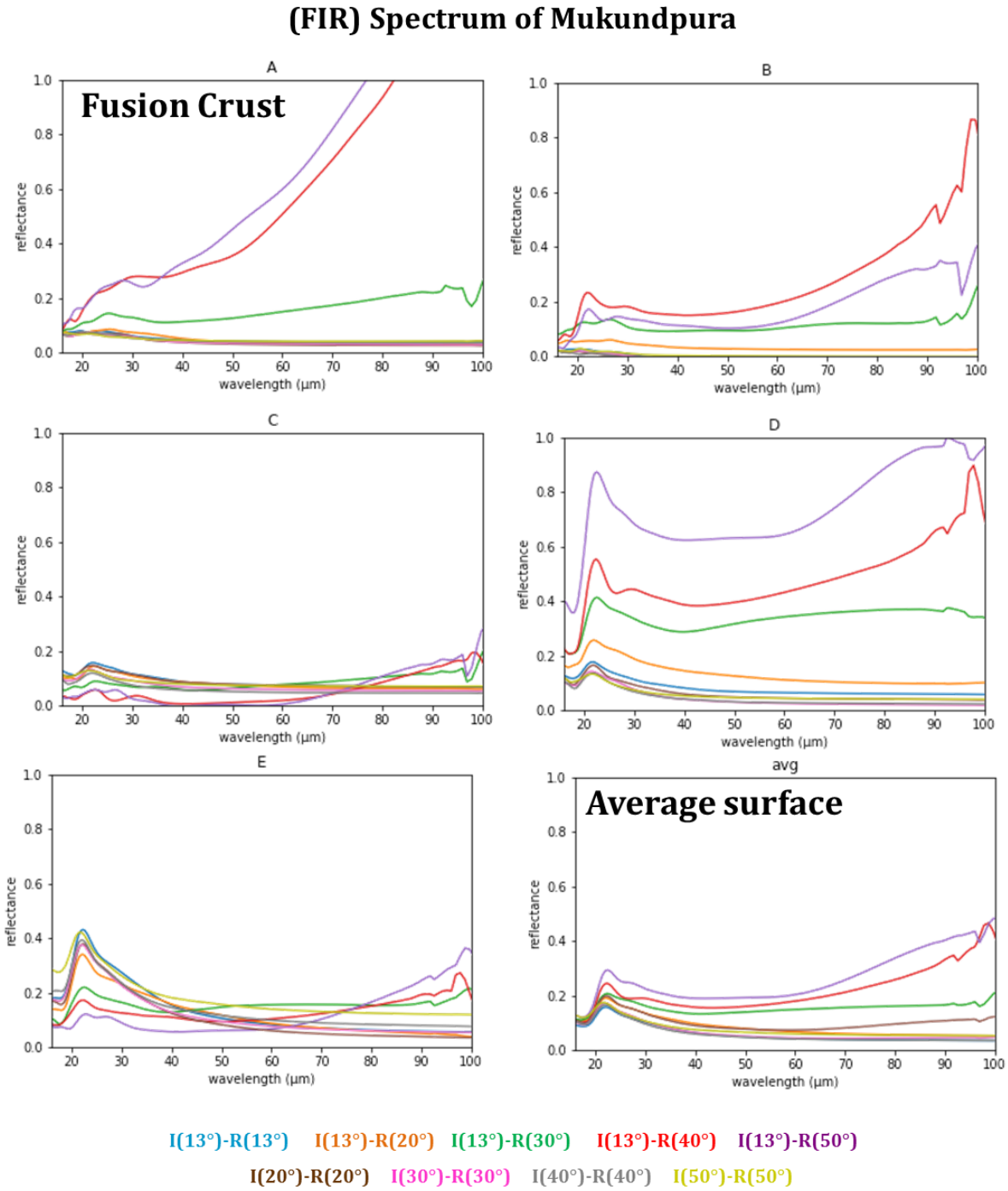

Figure 8. FIR spectra of fusion crust (A), intrinsic surfaces (B-E), and the average spectra of surafces (B-E) for its varying viewing geometry

Surfaces B-E (Fig. 8B-E): Irrespective of phase angle and surface roughness, all FIR spectra in the 16-60 μm spectral range have two characteristic spectral features of CM meteorites; a minor reflectance peak near 16 μm attributable to the librations of Mg-OH molecules within the octahedral sheet of 1:1 phyllosilicates [*Farmer*, 1974] and a sharp reflectance peak centered near ~22 μm corresponds to the bending modes of SiO_4 [*Farmer*, 1974;

Haberle et al., 2019]. These two distinct spectral features strongly indicate the presence of abundant Mg-serpentine within Mukundpura, which is also observed in the study by *Haberle et al.* [2019].

Fusion Crust A (Fig. 8A): The two spectral features centered near 16 μm (absorption) and 22 μm (peak) are highly subdued in the FIR spectra of the fusion crust (Fig. 8A), indicating the dehydration/loss of volatiles during the atmospheric entry of the meteorite fall. Also, the FIR spectra of fusion crust at phase angles 13º-40º (Fig. 8A; red) and 13º-50º (Fig. 8A; violet) display very strong redder spectral slope after 30 μm. In the remaining phase angle combinations, the spectra are nearly flat and dark.

5 Discussions

5.1 UV-FIR spectroscopy of Mukundpura

5.1.1 Mineralogy

Irrespective of the surface roughness and viewing geometry, all Mukundpura surfaces have characteristic spectral features that help us in deciphering their bulk mineralogy.

In the UV-VIS region (0.25 – 0.6 μm), both fusion crust (Fig. 4A) and the meteorite surfaces (Fig. 4B-E) exhibits carbon Fresnel peak (sp^2 π–π^*) near 0.275 μm [*Applin et al.,* 2018] along with flat spectra in the visible region 0.325-0.6 μm with reflectance values less than 0.1 for all surfaces indicating the presence to nanophase graphite or amorphous carbon in the matrix [*Applin et al.,* 2018].

In the VIS-IR region (0.4 – 1.0 μm; Fig. 5), the fresh interiors of Mukundpura sample for surface B have a minor absorption feature near 0.7 μm (attributable to Fe^{2+}-Fe^{3+} charge transfer) and amount of water within the CM and a downturn after 0.88 μm (ascribable to Fe^{2+} d-d crystal field transitions) indicating the presence of Fe-poor serpentines in the matrix [*Cloutis et al.,* 2011]. However VIS-IR spectra of surfaces C-E have evident IR downturn after 0.88 μm with weak or no 0.7 μm absorption features and may correspond to the surface containing bulk representation of matrix and chondrules containing crystalline anhydrous minerals (possibly Fe-bearing olivine within the chondrules) along with Fe-poor serpentines within the matrix [*Cloutis et al.,* 2011]. VIS-IR spectra of the fusion crust having a concave shape extending the entire VIS-IR spectral region with no absorption at 0.7 μm indicates the loss of water due to atmospheric heating and back-transformation of hydrous mineralogy to their anhydrous counterparts.

NIR spectral region (1.5-5 μm) of fresh interiors of all Mukundpura surfaces (Fig. 6; B-E) have the fundamental asymmetric spectral absorption feature associated with the hydroxyl (OH-) band centered at 2.72 μm supporting the presence of Mg-serpentines in its matrix. NIR spectra of the fusion crust also possess the weak 3 μm band centered near 2.7 μm indicating the potential survivability of some hydrous mineralogy within the matrix.

MIR spectral region (5-16 μm) of fresh Mukundpura surfaces (B-E) in Fig. 7 show that all the internal Mukundpura surfaces exhibit the characteristic CF minimum indicative of fundamental stretching modes of SiO_4 with their band center at 9 μm followed by reflectance peak near 16 μm indicator of librations of Mg-OH bonds. This further confirms the presence of Mg-rich serpentines in their matrix. The fusion crust spectra however exhibit the CF minimum slightly short-ward to 9 μm with very weak 16 μm peak, which indicates the formation of anhydrous minerals.

All FIR spectra (16-100 μm) of the intrinsic Mukundpura surfaces (Fig. 8; B-E) have the sharp reflectance peak near 22 μm which is the fundamental bending modes of SiO_4 in the aqueously altered minerals which is associated with the stretching modes of SiO_4 in the MIR

spectral region. FIR spectra of the fusion crust also possess the 22 μm spectral but weaker and broader indicating the presence of preferably anhydrous counterparts of Mg-serpentines such as Mg-olivine and pyroxene.

Overall, the carbon rich matrix along with the dominant presence of Mg-serpentines can be interpreted from the spectroscopy of the studied Mukundpura sample, along with the thermal alteration effects in the spectra of the fusion crust. Mukundpura sample studied appears to have very homogeneous bulk mineralogy for all the intrinsic surfaces.

5.1.2 Dependency on Viewing Geometry

The observations by Hayabusa2 and OSIRIS-REx show that the surfaces of both Ryugu and Bennu are not covered by regolith or fine dust but instead rocks of size similar to our Mukundpura fragment. This makes our study on viewing geometries especially relevant, as in the past typically all similar studies have been performed on powders.

This study shows that the spectral parameters such as brightness, slope, and absorption band centers of CM-type Mukundpura meteorite is highly influenced by the respective viewing geometry but behaves systematically for the respective spectral range irrespective of the 3D surface roughness for the compositionally homogeneous surface. In order to understand the general CM/Mukundpura spectral characteristics with respect to symmetrically and asymmetrically changing viewing geometry, the behavior of spectral parameters of average surface of Mukundpura is plotted against the varying geometry in Fig. 9.

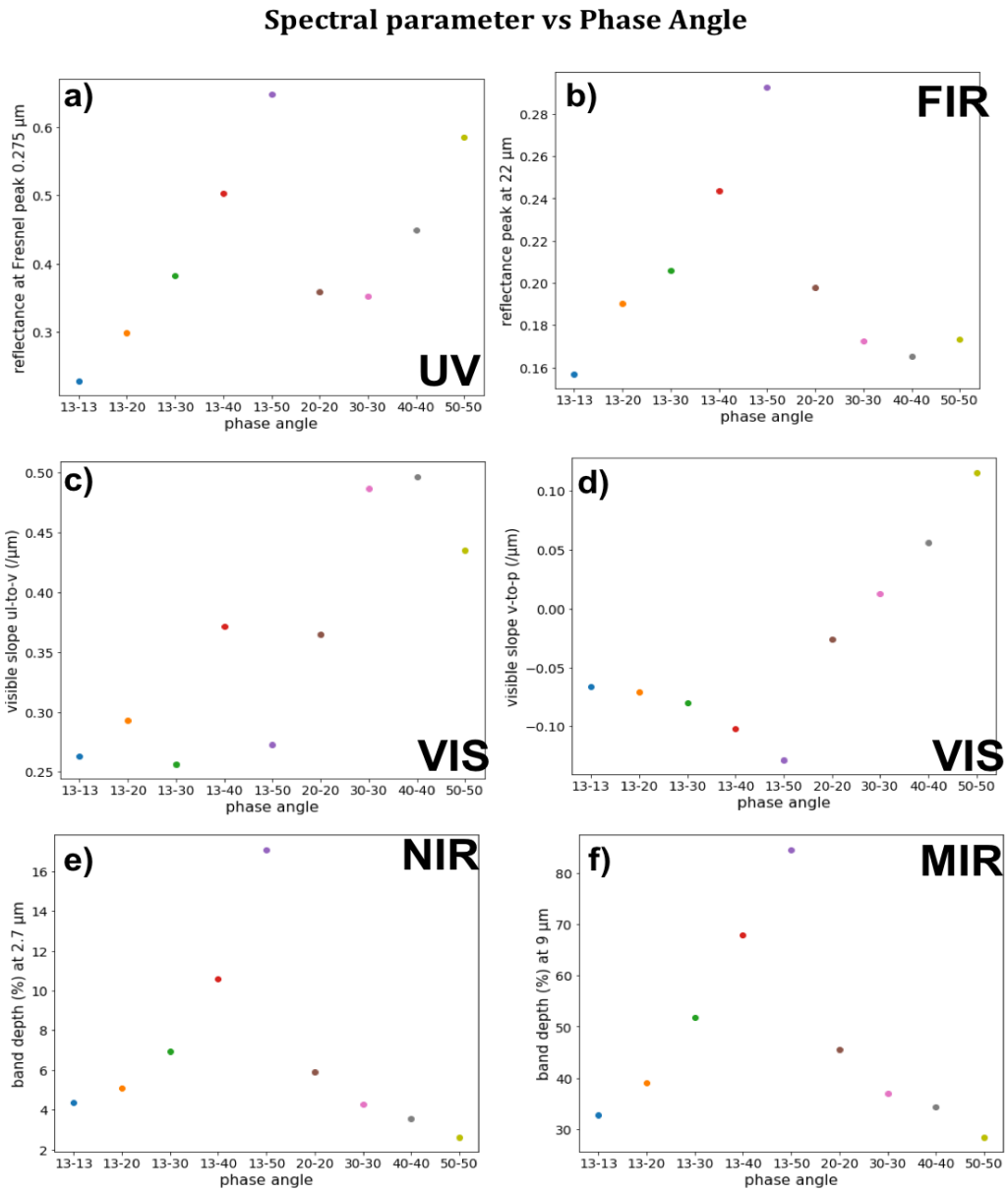

Figure 9. Relationship between symmetric and asymmetrically varying phase angle behavior with respect to UV-FIR spectral parameters derived from average surface spectra of Mukundpura meteorite studied; a) phase angle vs reflectance at UV fresnel peak of average surface spectra in Fig. 4, b) phase angle vs FIR reflectance peak at bending modes of SiO2 of average surface spectra in Fig. 8, c) phase angle vs VIS slope (ul-to-v) from average surface spectra in Fig. 5, d) phase angle vs VIS slope (v-to-p) from average surface spectra in Fig. 5, e) phase angle vs NIR band depth of water band at ~2.8 µm measured from average surface spectra in Fig. 6, and f) phase angle vs MIR band depth of reflectance minimum at ~9 µm measured from average surface spectra in Fig. 7.

UV-VIS spectral region (0.25 – 0.6 µm): Fig, 9a shows that for both asymmetrically and symmetrically increasing viewing geometries, the reflectance value at Fresnel peak near ~0.275 µm increases with increasing phase angle. It is also important to note that, the viewing geometry

with similar reflectance angle irrespective of the incidence angle have similar reflectance values at Fresnel peak (except for angle 20°-20°). It can be summarized as the reflectance value at the carbon Fresnel peak (~0.275 μm) decreases with decreasing reflectance angle in the order; 13º-50º, 50º-50º) > (13º-40º, 40º-40º) > (13º-30º, 30º-30º) > (13º-20º, 20º-20º) > (13º-13º). Therefore, for the spectroscopy of CM-petrology type or any C-type asteroids surfaces in the UV spectral region, irrespective of the foot-print of observation which is influenced by varying incidence angles and 3D surface roughness, the reflectance value at the carbon Fresnel peak is only dependent on the viewing angle/reflectance angle.

VIS-IR spectral region (0.4 – 1.0 μm): The behavior of visible spectral slopes ul-to-v and v-to-p for symmetrically and asymmetrically varying viewing angles is shown in Fig. 9c and Fig. 9d respectively. Fig. 9cshows no particular correlation among the viewing geometries for spectral slope ul-to-v for both symmetrically and asymmetrically varying phase angles. Whereas spectral slope v-to-p shows a systematic behavior with changing viewing geometry, where slope decreases with asymmetrically increasing phase angle and increases with symmetrically increasing phase angles. It can also be safely interpreted as v-to-p slope is positive for symmetric phase angles and negative for asymmetric phase angles. Therefore, our analysis suggests that the viewing geometry should be carefully considered while interpreting the spectral slopes in the remotely sensed C-type asteroids such as ONC-T data of Ryugu surface.

NIR & MIR spectral region (1.5 – 16.0 μm): In the NIR region, the 3 μm hydroxyl (OH-) absorption band is the characteristic spectral feature of C-type asteroids which indicates the nature and abundance of aqueously altered minerals in the surface. Whereas in the MIR region, the CF minimum is the characteristic spectral feature of CMs to characterize the nature and crystallinity of the silicate mineralogy. The band depth at 2.7 μm band and 9 μm absorption features for NIR and MIR spectral region is plotted in Fig. 9e and Fig. 9f for the symmetrically and asymmetrically varying viewing geometry. Fig. 9e, f shows that the band depths of these spectral absorption show similar behavior where the slope increases with asymmetrically increasing phase angle and decreases with symmetrically decreasing phase angles.

The absorption band depth significantly increases with increasing phase angles for the asymmetric viewing geometry in the order 13º-13º < 13º-20º < 13º-30º < 13º-40º < 13º-50º could be explained by spectral mixing of different minerals having different phase curves near 3 μm absorption band and 9 μm absorption band for the particular footprint/surface within the CM chondrite studied (as incidence angle is fixed). For asymmetric phase angles with fixed incidence angle, at low phase angles, the strong contributions from most materials is reflected and therefore weakens the absorption band. Whereas at higher phase angles the materials with lesser reflectance at large scattering angles do not contribute to the reflected signal and therefore enhances the absorption depth of 3 μm and 9 μm band. This may suggest that the water band and CF band for the hydrous minerals within the CMs is not affected by viewing geometry. This explanation is further supported by absolute reflectance of the spectra for all surfaces of the meteorite studied in Fig. 6i where the overall NIR reflectance of the spectra decreases with increasing phase angle for the asymmetric viewing geometry for all surfaces which is a reverse behavior to the absorption band center at 3 μm. This behavior can be traced for the overall MIR reflectance spectra in Fig. 7i. However, the absorption band strength for symmetric viewing geometry decreases with increasing phase but not significantly (Fig. 9 e, f). Also, the overall reflectance of the absolute spectra for all the surfaces for symmetric viewing geometry does not vary significantly (Fig. 6i; NIR and Fig. 7i; MIR). For all the surfaces the absorption band

strength for both 3 µm (Fig. 6iii, Fig. 9e) and 9 µm (Fig. 7ii, Fig. 9f) absorption band is largest for viewing geometry 13º-50º and is least for viewing geometry 50º-50º.

FIR spectral region (16 – 100 µm): The FIR spectral behavior with respect to viewing geometry is highly influenced by the respectively surface roughness and texture (Fig. 8). In order to understand the general FIR spectral characteristics for varying viewing geometry, the reflectance peak near 22 µm for average surface spectra is plotted against the symmetrically and asymmetrically varying viewing geometry in Fig. 9b. Fig. 9b shows that the reflectance peak near 22 µm increases with increasing asymmetrically varying viewing geometry. However, this behavior at first decreases with decreasing symmetrically varying geometry and then increases. The absolute spectra in Fig. 8 shows that the large phase angles in the asymmetric viewing geometry especially 13º-40º (Fig. 8; red) and 13º-50º (Fig. 8; violet) shows a broad absorption band extending from 22 to 100 µm.

5.1.3 Dependency of 3D surface roughness

Throughout the study, it is evident that all internal Mukundpura surfaces (B-E) for all spectral regions from UV-FIR preserve their characteristic band absorption centers irrespective of the differences in the viewing angle and the surface roughness for the corresponding spectral region such as

a) Fresnel peak for carbon in UV region (Fig. 4), 0.7 µm feature weak or null indicating the presence of Fe-poor phyllosilicates in the VIS-IR region (Fig. 5),
b) fundamental OH- absorption featured centered at 2.72 µm indicating the presence of Mg-serpentine in the NIR spectral region (Fig. 6),
c) fundamental stretching and bending modes of SiO_4 near 9 µm and 22 µm respectively along with the reflectance peak near 16 µm indicating Mg-OH librations in phyllosilicates which further confirming the presence of volumetrically abundant Mg-rich phyllosilicates such as Mg-serpentines within Mukundpura bulk mineralogy in the mid-far IR spectral region (MIR in Fig. 7 and FIR in Fig. 8).

Overall, it can be confidently stated that Mukundpura sample obtained has homogeneous bulk mineralogy for all the intrinsic surfaces.

Varying viewing geometry either symmetrically and asymmetrically exhibit characteristic trends in the spectral parameters such as spectral slopes (VIS-IR in Fig. 5) and absorption band depths (NIR in Fig. 6 and MIR in Fig. 7) for the corresponding spectral region depending on the mineralogical indicator (See Section 5.1.2) for each of the respective surface.

Yet, each internal surface of Mukundpura differs in the nature of their absolute spectral shape and overall reflectance value variations for a fixed viewing angle throughout the spectral range (UV-FIR). This difference is attributed to the 3D roughness of the surface itself and its variation for different surfaces (Fig. 1b-h). The resulting spectral shape for a fixed viewing angle for all intrinsic surfaces (B-E) is influenced by their respective roughness which defines the number and area of different reflecting/sloping faces and their corresponding reflecting angles with respect to the direction of the incident light.

This compels us to be careful while performing spectral parameter analysis of the remotely sensed data of rough and rocky surface target such as Ryugu and Bennu which has boulder-filled rough terrains with basically no smooth regions.

5.2. Application to Hayabusa 2 & OSIRIS-REx

For comparison, Mukundpura's fusion crust (surface A) spectra (Fig. 10; gray) and the average surface (average of surfaces B-E) spectra (Fig. 10; black) for viewing geometry 13º-20º is chosen to compare with the remotely sensed spectra of Ryugu (Fig. 10; red) and Bennu (Fig. 10; blue) for the respective spectral region, VIS-IR (Fig. 10a), NIR (Fig. 10b), and thermal-infrared (TIR; Fig. 10c,d).The spectra of Ryugu and Bennu for its respective spectral range shown in Fig. 10 are obtained by extracting the published spectral data by *Kitazato et al.* [2019], *Tatsumi et al.* [2019] and *Hamilton et al.* [2019] respectively using an online tool, WebPlotDigitizer (https://automeris.io/WebPlotDigitizer/).

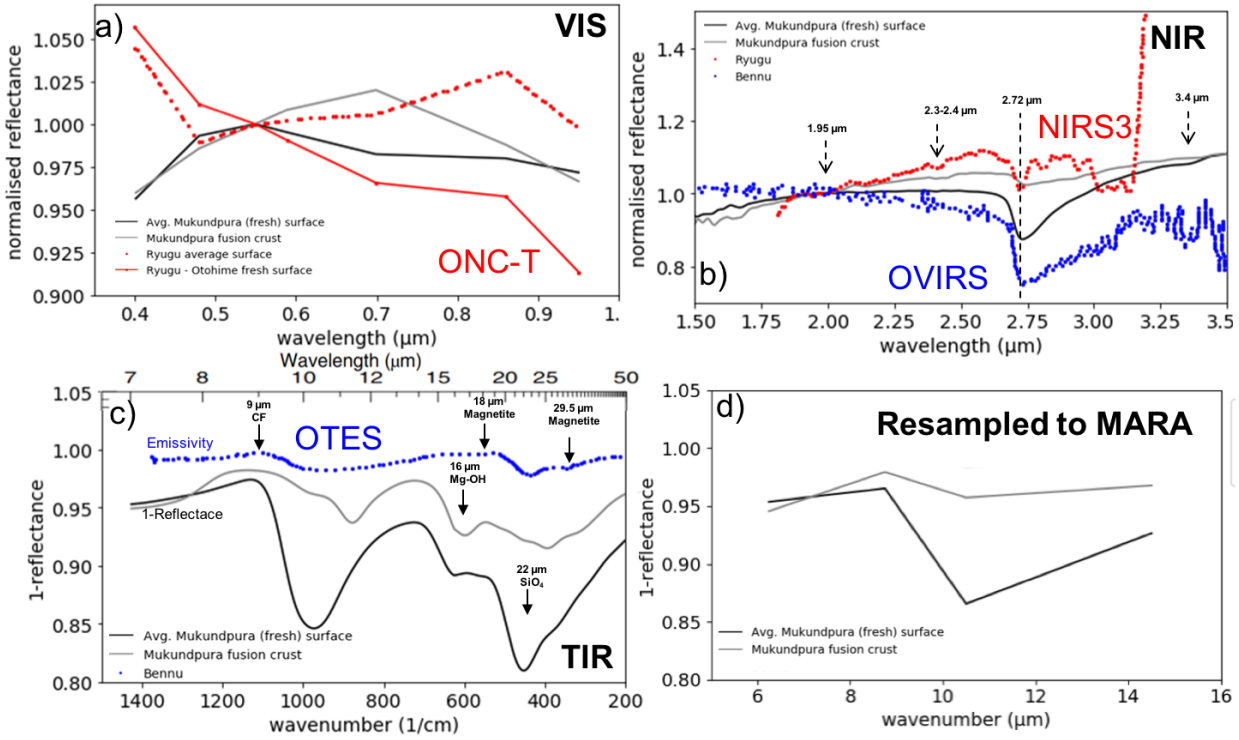

Figure 10. Comparison of Mukundpura fusion crust and average intrinsic surface spectra compared with the extracted Ryugu and Bennu spectra [*Kitazato et al.*, 2019; *Tatsumi et al.*, 2019] and [*Hamilton et al.*, 2019] respectively using an online tool, WebPlotDigitizer (https://automeris.io/WebPlotDigitizer/). a) VIS-IR region; Mukundpura vs ONC-T data of Ryugu for its average surface and fresh Otohime surface, b) NIR region spectra of Mukundpura, Bennu (from OVIRS), and Ryugu (NIRS3), and c) MIR region; Mukundpura vs Bennu from OTES, d) Mukundpura fusion crust and average intrinsic surface spectra resampled to MARA-TIR bands.

5.2.1 Hayabusa2/ONC-T in 0.4-1 µm

ONC-T data shows that Ryugu's surface is covered by numerous boulders (number density twice as that of Itokawa) of scale-invariant varying brightness; where brighter boulders are associated with smooth and layered surface and the darker boulders are associated with rugged and crumbling rough surface [*Sasaki et al.*, 2019]. These differences in brightness is contributed mainly by degrees of space weathering but less contributed by compositional variations [*Sasaki et al.*, 2019].

744 The spectral characterization of various boulders across Ryugu surface using ONC-T data
745 by [*Tatsumi et al.,* 2019] shows that fresh surfaces show blue spectra and while exposed to space
746 weathering processes, the spectra reddens. This conclusion is supported by studying the spectral
747 nature of two faces of the largest boulder Otohime Saxum (~140 m), one which is moderately
748 sloped face whose spectra is comparable to the average Ryugu spectra (Fig. 10a; red-dotted line)
749 and the other is cliff-like face which could have formed by recent impacts or landslides shows
750 bluer spectra (Fig. 10a; solid-red) [*Tatsumi et al.,* 2019]. The Ryugu spectra, both average and
751 Otohime spectra, plotted in Fig. 10a is extracted from [*Tatsumi et al.,* 2019].
752 Tatsumi et al. (2019) also studied the spectral parameters such as spectral slope v-to-p
753 slope ($Ref_{0.55}/R_{0.95}$) and ul-to-v slope ($Ref_{0.40}/Ref_{0.55}$). All Ryugu spectra have ul-band upturn,
754 0.40 μm upturn, (Fig. 10a; red-dotted line) and this value vary among boulders of varying sizes
755 and relates to atleast two different processes on Ryugu's surface; one which affects the spectral
756 slopes could be related to space weathering [*Ivanova et al.,* 2010; *Lantz et al.,* 2017; *Nakamura,*
757 2005] and the other which affects the ul-band upturn could correspond to degree of aqueous
758 alteration [*Hiroi et al.,* 1996] and/or the presence of carbon contents [*Hendrix et al.,* 2016].
759 However, Mukundpura spectra for both fusion crust (Fig. 10a; gray) and the interior surfaces
760 (Fig. 10a; black) have ul-band downturn. The average surface spectra in Fig. 10a for
761 Mukundpura represents the mineralogy of interior which is devoid of any space weathering such
762 as solar wind irradiation and micro-meteorite impacts and solar radiation heating processes.
763 Though fusion crust is thermally altered, it is still devoid of signatures of prolonged space
764 weathering processes as they are lost during the atmospheric entry. This may suggest that ul-
765 upturn of Ryugu spectra may represent the space weathering processes; however, the differences
766 in degree of aqueous alteration and presence of carbon content from Mukundpura should be
767 considered.
768 The average intrinsic Mukundpura VIS-IR spectra (Fig. 10a; black) after 0.55 μm
769 behaves similar to the fresh Otohime surface with the blue-sloped (negative-sloped) spectra with
770 minor absorption band around 0.7 μm and absorption band after 0.88 μm; however, the degree of
771 slope for fresher Ryugu spectra is slightly bluer than that of fresh Mukundpura surface.
772 Overall, the fusion crust spectra of Mukundpura spectra as a concave-shape with the
773 reflectance maximum at 0.7 μm which confirms the loss of water due to atmospheric heating and
774 the absorption feature after 0.7 μm may further indicate the presence of anhydrous minerals
775 which is dehydrated from their hydrous counterparts. It is also important to note the reddening of
776 the fusion crust spectra relative to the intrinsic Mukundpura surfaces up to 0.7 μm. The slope of
777 the fusion crust and Ryugu spectra in 0.55-0.7 μm is comparable. Thus, the reddening of the
778 Ryugu spectra in relative to the fresh Otohime surface could be explained by solar radiative
779 heating in its past.
780
781 **5.2.2 Hayabusa2/NIRS3 and OSIRIS-REX/OVIRS in 1.5-3.5 μm**
782 *Kitazato et al.* [2019] study shows that the thermally and radiometrically calibrated
783 spectral data from NIRS3/Hayabusa2 reveals that near-infrared (NIR) reflectance spectra of
784 entire Ryugu exhibit a spectrally 'red' (positive) continuum slope spectra with a weak, narrow
785 absorption feature centered at 2.72 μm indicating the presence of OH-bearing minerals, most
786 likely Mg-rich phyllosilicates throughout the surface. The study [*Kitazato et al.,* 2019] also
787 suggests that intensity of 2.72 μm band has positive correlation with estimated surface
788 temperature but when normalized for observed temperature, the intensity of 2.72 μm shows no
789 correlation with topographic/morphologic features. The absorption strength of this band for the

normalized NIRS3 spectra ranges from 7-10%. This weak OH absorption feature and dark surface of Ryugu is attributed to either or all of the following conditions; early geologic history where inherent chemical composition with low water/rock ratio, and ongoing processes such as solar radiative heating during close approach to Sun and continuous space weathering processes such as solar-wind irradiation and micrometeorite impacts [*Kitazato et al.,* 2019]. The proposed possible compositional analogues of Ryugu are CMs and CIs [*Le Corre et al.,* 2017; *Moskovitz et al.,* 2013; *Perna et al.,* 2017; *Vilas,* 2008].

On the other hand, OVIRS/OSIRIS-REx spectral data of Bennu analyzed by *Hamilton et al.* [2019] exhibits spectrally "blue" (negative) continuum slope comparable to telescope data by *Clark et al.* [2011] along with the stronger 2.7 μm OH-absorption feature centered around 2.74 ± 0.01 μm for all OVIRS spectra and corresponds to meteorites having petrologic types of CM2.1-2.2 those have absorption band centers at 2.72 μm [*Takir et al.,* 2013]. *Hamilton et al.* [2019] stresses that though negative or blue spectral slope of carbonaceous materials could be attributed to space weathering [*Brunetto et al.,* 2014; *Lantz et al.,* 2018; *Thompson et al.,* 2019], there is no sufficient information to confidently attribute the spectral slope of Bennu to space weathering or the presence of fine-particulate magnetite and/or insoluble inorganic material, however, the detailed analysis of high spatial resolution OVIRS data will further help us to draw conclusions.

In order to compare the NIR spectra of Ryugu and Bennu with our studied CM-type Mukundpura rock, we first extracted spectra of NIRS3/Ryugu from Fig. 1B of Kitazato et al. (2019) and OVIRS/Bennu spectra from Fig.1 of Hamilton et al. (2019). We then normalized the NIR spectra of Ryugu (Fig. 10b; red), Bennu (Fig. 10b; blue), the fusion crust (surface A) and average surface spectra (average spectra of surfaces B,C,D,E) of Mukundpura for viewing geometry 13º-20º as it closely corresponds to nadir viewing of NIRS3 (Fig. 10b; gray and blue respectively) to a reflectance value of 1.0 at 2 μm as shown in Fig. 10b.

NIR spectral slope: For the spectral region 1.5-2.7 μm, the slope of the normalized NIR spectra (Fig. 10b) of average Mukundpura surface spectra (Fig. 10b; black) is nearly flat and unlike red-sloped Ryugu spectra (Fig. 10b; red) and blue-sloped Bennu spectra (Fig. 10b; blue). However, the fusion crust spectra (Fig. 10b; gray) have slightly redder slope compared to the fresh Mukundpura surface (Fig. 10b; black). This suggests that the reddening of the NIR continuum spectra of Mukundpura is caused by the thermal weathering of fusion crust during the path of meteorite fall. The redder slope of Ryugu spectra (Fig. 10b; red) could therefore be associated to heating of Ryugu either by solar radiative heating during shortened perihelion distances in its past [*Kitazato et al.,* 2019].

NIR absorption bands: Fig. 10b shows that Bennu's OVIRS spectrum (Fig. 10b; blue) has the strongest and broad asymmetric 2.7 μm absorption band compared to Mukundpura and Ryugu NIR spectra. The average surface spectrum of Mukundpura (Fig. 10b; black) has comparatively weaker absorption feature centered at 2.72 μm with an asymmetric spectral shape. However, NIR spectrum of fusion crust of Mukundpura has the highly subdued, broader asymmetric OH-absorption feature with its center slightly moved longward from its average surface spectrum, centered at 2.74 μm similar to Bennu spectrum. On the other hand, Ryugu spectrum shows the weak but sharp symmetric OH-absorption feature centered at 2.72 μm. Nevertheless, in the shorter wavelengths (1.75-2.5 μm), both fusion crust of Mukundpura (Fig. 10b; gray) and Ryugu (Fig. 10b; red) share significantly similar spectral shape with spectral features such as; a) a minor absorption band in 2.3-2.4 μm region which is characteristic spectral feature of metal-OH bond in serpentines [*Cloutis et al.,* 2011], and the minor broad absorption bands near 1.95 μm with spectral shoulders near 1.9 μm and 2.08 μm (Fig.9b); and these features

are not prominent in the fresh average surface spectra of Mukundpura. *Kitazato et al.* [2019] mentioned that no existing meteorite samples reflectance spectra matches with Ryugu visible to NIR wavelength. Our results reveal the intrinsic (B-E) surface of Mukundpura shows fundamental absorption as 2.72 μm with an additional shared band absorption near 1.95 μm and 2.3-2.4 μm. Even the fusion crust hosts considerable absorption at this wavelength. Thus, thermally metamorphosed and shocked Mukundpura with diagnostic 2.72 μm absorption is highly comparable to the Ryugu. Therefore, supporting that Ryugu surface has experienced extensive heating in its geologic past.

Overall reddening of spectral shape of fusion crust with similar spectral shape near 1.95, 2.3-2.4 μm, and weak 2.7 μm band as Ryugu could explain the heating of Ryugu surface in its history. However, the strong asymmetric 2.72 μm band of Mukundpura internal surface resembling Bennu spectrum suggests that Bennu has not undergone significant heating compared to Ryugu. In addition to this, the 3.4 μm absorption band corresponding to presence of organics suggested for Bennu [*Lauretta et al.,* 2019] can be traced in the average surface spectra of Mukundpura in Fig. 10b which is much evident in the continuum removed spectra in Fig. 6iii suggesting the presence of organics in the fresh Mukundpura surface, however, this feature is much subdued in the fusion crust spectra (Fig. 10b).

5.2.3 OSIRIS-REX/OTES in7-50 μm

OTES spectrometer onboard OSIRIS-Rex maps the emissivity spectrum of Bennu at the spectral range 7-50 μm. *Hamilton et al.* [2019] shows that calibrated average disk integrated spectrum of Bennu exhibits the CF position similar to that of the CM1/2 and CM2 petrologic types which is the emissivity maximum around 9 μm indicating the presence of stretching modes of SiO_4 in the hydrous silicates. To compare Mukundpura spectra with Bennu's OTES/OSIRIS-REx spectra, we first extracted the calibrated disk-integrated average emissivity spectrum of Bennu from Fig. 3 of *Hamilton et al.* [2019]. Bennu spectrum also exhibits the absorption feature near 22 μm indicative of the presence of corresponding bending modes of SiO_4 in the hydrous silicates. In addition to that, OTES spectrum of Bennu spectrum also exhibits the spectral indicators of presence of magnetite which includes the minor absorption bands near 18 μm and 29.5 μm. OTES data analyzed by *Hamilton et al.* [2019] also shows that entire Bennu surface is spatially uniform at 80 m spatial scale with similar range of particle sizes for each pixel at large spatial scales.

In order to compare the emissivity spectrum of Bennu with the measured reflectance of Mukundpura surface and fusion crust (Fig. 10c), we estimated 1-reflectance of Mukundpura spectra as a proxy for emissivity (Kirchoff's law). Bennu's OTES spectrum (Fig. 10c; blue) resembles the average Mukundpura surface (Fig. 10c; black) except for the lack of characteristic Mg-OH band near 16 μm which is the indicator of Mg-serpentines of Mukundpura. As suggested by *Hamilton et al.* [2019], the lack of this 16 μm feature could be attributed to presence of non-Mg endmember (possibly Fe-bearing phyllosilicates), modest heating, disorder and/or particle sizes. However, thermally altered Mukundpura which has indicators of loss of water in the VIS-NIR spectral region, still preserves the 16 μm Mg-OH absorption band (Fig. 10c).

Our spectral analysis revealed that both Bennu and Mukundpura surface has CF band near 9 μm and the absorption band near 22 μm suggestive of the hydrous minerals. This suggests that Bennu surface is volumetrically dominated by the phyllosilicates and therefore indicating the aqueous alteration of the parent body. However, OTES spectrum of Bennu possess lesser spectral contrast compared to average Mukundpura spectrum (Fig. 10c; black) especially in the

regions of silicate stretching bands (9-14.5 μm) where Bennu spectrum exhibits a broader, bowl-like shape unlike the sharp distinct transparency features resulting from volume scattering in the case of average Mukundpura surface. This may indicate that Bennu's surface is dominated by amorphous/disordered component [*Hamilton et al.,* 2019] unlike ordered/crystalline Mukundpura interior surface and attribution of this amorphous/disordered behavior to the lack of 16 μm should be studied further. 18 μm absorption feature corresponding to magnetite can be traced for a weak absorption for Mukundpura for its average fresh surface.

The 1-reflectance TIR spectra of fusion crust (Fig. 10c; gray) exhibits sharp-fine 12 μm feature with minor absorption bands around 10.6 μm, 11.4 μm, and 12.4 μm indicative of the back-transformation of hydrous minerals to their corresponding anhydrous silicates, olivine and pyroxene [*Beck et al.,* 2018]. The overall shape of fusion crust in TIR spectral region is different from that of Bennu's spectrum which further confirms that Bennu's surface is dominated by the aqueously altered minerals.

5.2.3 Hayabusa2/MASCOT/MARA in 5-16μm

Hayabusa2 also carried two surface spectrometers with the DLR's MASCOT lander; 6-band thermal radiator (MARA) and a hyperspectral infrared microscope (MicrOmega). MARA houses 4 bandpass spectral channels in the range of 5.5–7 μm, 8–9.5 μm, 9.5–11.5 μm, and 13.5–15.5 μm, as well as one long-pass channel sensitive in the >3 μm range [*Grott et al.,* 2017]. In Fig. 10d, the average fresh surface and fusion crust of Mukundpura and Bennu OTES spectra is resampled to MARA spectral bands. This will further help MARA data analysis to be compared with Mukundpura as a Ryugu's analogue.

6 Conclusions

In this work, the ultraviolet to far-infrared reflectance spectra of extremely fresh carbonaceous chondrite rock (Mukundpura meteorite) have been studied for symmetrically and asymmetrically varying viewing geometries. The comparison of the spectral behavior of the fusion crust to the fresh interiors further helps to understand the evolution of the spectral behavior due to thermal alteration during atmospheric entry. The systematic spectral behavior trend in the reflectance of CM chondrites (Mukundpura with intrinsic and fusion crust) in Fresnel peak in UV, visible-IR slope after 0.55 μm, fundamental hydroxyl (OH-) band strength in NIR and the Christiansen Feature minimum at MIR with symmetric and asymmetric varying geometry is observed for the first time. The change in overall reflectance value and the spectral shape due to changes in 3D surface roughness is observed in the study. In addition to photometric corrections which corrects for viewing geometry, the significant spectral effects due to the varying 3D roughness of the rocky boulder-like terrain of Ryugu and Bennu should be carefully considered while attempting to quantify the mineralogy interpretations such as amount of water, magnetite, carbon, hydrous minerals etc for their corresponding spectral regions. The phase angle/viewing geometry dependent UV-FIR reflectance spectroscopy of fresh CM rock reveals that the fundamental absorption band centers at all wavelengths are not (or least) affected by surface roughness and viewing geometry; however, their band strengths and spectral band shape varies.

The results reveal that the thermally metamorphosed and shocked Mukundpura fusion curst with diagnostic 2.72 μm absorption is comparable to the Ryugu. Therefore, supporting that Ryugu surface has experienced extensive heating in its geologic past. The asymmetric 3 μm band of Bennu is significantly comparable to the strong asymmetric absorption band of intrinsic

Mukundpura surfaces, which further supports that Bennu's upper layer had not undergone heating compared to Ryugu surface. Instead of powdered samples of meteorites, the direct spectral investigation of varying surface roughness of single Mukundpura sample under varying viewing geometry therefore potentially support the spectral analysis of Ryugu and Bennu spectral data from orbit and surface and future exploration of C-type asteroids.

Acknowledgements

The authors thank DLR/DAAD Doctorate Fellowship to Indhu Varatharajan for funding her PhD work at PSL-DLR. A portion of this research was supported by the European Union's Horizon 2020 research and innovation program. Europlanet 2020 RI has received funding from the European Union's Horizon 2020 research and innovation programme under grant agreement No 654208. The work at PRL is supported by Department of Space, Government of India.

References

Anders, E., and N. Grevesse (1989), Abundances of the elements: Meteoritic and solar, Geochimica et Cosmochimica Acta, 53(1), 197-214, doi:https://doi.org/10.1016/0016-7037(89)90286-X.

Applin, D. M., M. R. M. Izawa, E. A. Cloutis, J. J. Gillis-Davis, K. M. Pitman, T. L. Roush, A. R. Hendrix, and P. G. Lucey (2018), Ultraviolet spectral reflectance of carbonaceous materials, Icarus, 307, 40-82, doi:https://doi.org/10.1016/j.icarus.2018.02.012.

Baliyan, S., and D. Ray (2019), Colour Cathodoluminescence study of forstertic Olivine in Mukundpura (CM2) meteorite, 50th Lunar and Planetary Science Conference, Abstract #1603.

Barber, D. J. (1981), Phyllosilicates and other layer-structured minerals in stony meteorites, Clay Miner., 20, 415–454.

Barrat, J. A., B. Zanda, F. Moynier, C. Bollinger, C. Liorzou, and G. Bayon (2012), Geochemistry of CI chondrites: Major and trace elements, and Cu and Zn Isotopes, Geochimica et Cosmochimica Acta, 83, 79-92, doi:https://doi.org/10.1016/j.gca.2011.12.011.

Beck, P., A. Garenne, E. Quirico, L. Bonal, G. Montes-Hernandez, F. Moynier, and B. Schmitt (2014), Transmission infrared spectra (2–25μm) of carbonaceous chondrites (CI, CM, CV–CK, CR, C2 ungrouped): Mineralogy, water, and asteroidal processes, Icarus, 229, 263-277, doi:https://doi.org/10.1016/j.icarus.2013.10.019.

Beck, P., A. Maturilli, A. Garenne, P. Vernazza, J. Helbert, E. Quirico, and B. Schmitt (2018), What is controlling the reflectance spectra (0.35–150 μm) of hydrated (and dehydrated) carbonaceous chondrites?, Icarus, 313, 124-138, doi:https://doi.org/10.1016/j.icarus.2018.05.010.

Beck, P., et al. (2010), Hydrous mineralogy of CM and CI chondrites from infrared spectroscopy and their relationship with low albedo asteroids, Geochimica et Cosmochimica Acta, 74(16), 4881-4892, doi:https://doi.org/10.1016/j.gca.2010.05.020.

965 Browning, L. B., H. Y. McSween, and M. E. Zolensky (1996), Correlated alteration effects in
966 CM carbonaceous chondrites, Geochimica et Cosmochimica Acta, 60(14), 2621-2633,
967 doi:https://doi.org/10.1016/0016-7037(96)00121-4.

968 Brunetto, R., et al. (2014), Ion irradiation of Allende meteorite probed by visible, IR, and Raman
969 spectroscopies, Icarus, 237, 278-292, doi:https://doi.org/10.1016/j.icarus.2014.04.047.

970 Christensen, P. R., et al. (2018), The OSIRIS-REx Thermal Emission Spectrometer (OTES)
971 Instrument, Space Science Reviews, 214(5), 87, doi:10.1007/s11214-018-0513-6.

972 Clark, B. E., et al. (2011), Asteroid (101955) 1999 RQ36: Spectroscopy from 0.4 to 2.4μm and
973 meteorite analogs, Icarus, 216(2), 462-475, doi:https://doi.org/10.1016/j.icarus.2011.08.021.

974 Clark, R. N., T. V. V. King, and N. S. Gorelick (1987), Automatic continuum analysis of
975 reflectance spectra., In: Proceedings, Third AIS Workshop, 2–4 June, 1987, JPL Publication, 97-
976 130, 138–142.

977 Clark, R. N., and T. L. Roush (1984), Reflectance spectroscopy: Quantitative analysis techniques
978 for remote sensing applications, Journal of Geophysical Research: Solid Earth, 89(B7), 6329-
979 6340, doi:10.1029/JB089iB07p06329.

980 Cloutis, E. A., P. Hudon, T. Hiroi, M. J. Gaffey, and P. Mann (2011), Spectral reflectance
981 properties of carbonaceous chondrites: 2. CM chondrites, Icarus, 216(1), 309-346,
982 doi:https://doi.org/10.1016/j.icarus.2011.09.009.

983 DellaGiustina, D. N., et al. (2019), Properties of rubble-pile asteroid (101955) Bennu from
984 OSIRIS-REx imaging and thermal analysis, Nature Astronomy, 3(4), 341-351,
985 doi:10.1038/s41550-019-0731-1.

986 Farmer, V. C. (1974), The Infrared Spectra of Minerals, Mineralogical Society, London,
987 Monograph 4(331), doi:http://dx.doi.org/10.1180/mono-4.15.

988 Flynn, G. J., G. J. Consolmagno, P. Brown, and R. J. Macke (2018), Physical properties of the
989 stone meteorites: Implications for the properties of their parent bodies, Geochemistry, 78(3),
990 269-298, doi:https://doi.org/10.1016/j.chemer.2017.04.002.

991 Garenne, A., P. Beck, G. Montes-Hernandez, O. Brissaud, B. Schmitt, E. Quirico, L. Bonal, C.
992 Beck, and K. T. Howard (2016), Bidirectional reflectance spectroscopy of carbonaceous
993 chondrites: Implications for water quantification and primary composition, Icarus, 264, 172-183,
994 doi:https://doi.org/10.1016/j.icarus.2015.09.005.

995 Garenne, A., P. Beck, G. Montes-Hernandez, R. Chiriac, F. Toche, E. Quirico, L. Bonal, and B.
996 Schmitt (2014), The abundance and stability of "water" in type 1 and 2 carbonaceous chondrites
997 (CI, CM and CR), Geochimica et Cosmochimica Acta, 137, 93-112,
998 doi:https://doi.org/10.1016/j.gca.2014.03.034.

Glotch, T. D., G. R. Rossman, and O. Aharonson (2007), Mid-infrared (5–100 μm) reflectance spectra and optical constants of ten phyllosilicate minerals, Icarus, 192(2), 605-622, doi:https://doi.org/10.1016/j.icarus.2007.07.002.

Grott, M., J. Knollenberg, B. Borgs, F. Hänschke, E. Kessler, J. Helbert, A. Maturilli, and N. Müller (2017), The MASCOT Radiometer MARA for the Hayabusa 2 Mission, Space Science Reviews, 208(1), 413-431, doi:10.1007/s11214-016-0272-1.

GSI (2017), Preliminary Study Note on the Meteorite Fall at Mukundpura, Bhankrota, Jaipur, Official report from Geological Survey of India, Govt of India, Link: https://employee.gsi.gov.in/cs/groups/public/documents/document/b3zp/mtq4/~edisp/dcport1gsigovi148390.pdf.

Haberle, C. W., P. R. Christensen, L. A. J. Garvie, V. E. Hamilton, R. D. Hanna, H. C. C. Jr., D. S. Lauretta, and a. t. O.-R. Team. (2019), The Mineralogy of Recently Fallen Carbonaceous Meteorites, Mukundpura and Sutter's Mill, in the Context of Asteroid (101955) Bennu, 50th Lunar and Planetary Science Conference, Abstract #2144.

Hamilton, V. E., et al. (2019), Evidence for widespread hydrated minerals on asteroid (101955) Bennu, Nature Astronomy, 3(4), 332-340, doi:10.1038/s41550-019-0722-2.

Hanowski, N. P., and A. J. Brearley (2001), Aqueous alteration of chondrules in the CM carbonaceous chondrites, Allan Hills 81002. , Geochim. Cosmochim. Acta 65, 495–518.

Hendrix, A. R., F. Vilas, and J.-Y. Li (2016), The UV signature of carbon in the solar system, Meteoritics & Planetary Science, 51(1), 105-115, doi:doi:10.1111/maps.12575.

Hiroi, T., M. E. Zolensky, C. M. Pieters, and M. E. Lipschutz (1996), Thermal metamorphism of the C, G, B, and F asteroids seen from the 0.7 μm, 3 μm, and UV absorption strengths in comparison with carbonaceous chondrites, Meteoritics & Planetary Science, 31(3), 321-327, doi:doi:10.1111/j.1945-5100.1996.tb02068.x.

Howard, K. T., G. K. Benedix, P. A. Bland, and G. Cressey (2009), Modal mineralogy of CM2 chondrites by X-ray diffraction (PSD-XRD). Part 1: Total phyllosilicate abundance and the degree of aqueous alteration, Geochimica et Cosmochimica Acta, 73(15), 4576-4589, doi:https://doi.org/10.1016/j.gca.2009.04.038.

Howard, K. T., G. K. Benedix, P. A. Bland, and G. Cressey (2011), Modal mineralogy of CM chondrites by X-ray diffraction (PSD-XRD): Part 2. Degree, nature and settings of aqueous alteration, Geochimica et Cosmochimica Acta, 75(10), 2735-2751, doi:https://doi.org/10.1016/j.gca.2011.02.021.

Ivanova, M. A., C. A. Lorenz, M. A. Nazarov, F. Brandstaetter, I. A. Franchi, L. V. Moroz, R. N. Clayton, and A. Y. Bychkov (2010), Dhofar 225 and Dhofar 735: Relationship to CM2 chondrites and metamorphosed carbonaceous chondrites, Belgica-7904 and Yamato-86720, Meteoritics & Planetary Science, 45(7), 1108-1123, doi:doi:10.1111/j.1945-5100.2010.01064.x.

Izawa, M. R. M., V. Reddy, L. L. Corre, A. McGraw, J. A. Sanchez, E. A. Cloutis, K. Yamashita, A. P. Jephcoat, D. M. Applin, and B. J. Hall (2019), Discovery of a Possible CM2 Carbonaceous Chondrite Parent Body in the Nearearth Asteroid Population. , 50th Lunar and Planetary Science Conference, Abstract #3174.

Jacinto, A.-A., et al. (2013), UV to far-IR reflectance spectra of carbonaceous chondrites – I. Implications for remote characterization of dark primitive asteroids targeted by sample-return missions, Monthly Notices of the Royal Astronomical Society, 437(1), 227-240, doi:10.1093/mnras/stt1873.

Kitazato, K., et al. (2019), The surface composition of asteroid 162173 Ryugu from Hayabusa2 near-infrared spectroscopy, Science, eaav7432, doi:10.1126/science.aav7432.

Lantz, C., R. P. Binzel, and F. E. DeMeo (2018), Space weathering trends on carbonaceous asteroids: A possible explanation for Bennu's blue slope?, Icarus, 302, 10-17, doi:https://doi.org/10.1016/j.icarus.2017.11.010.

Lantz, C., R. Brunetto, M. A. Barucci, S. Fornasier, D. Baklouti, J. Bourçois, and M. Godard (2017), Ion irradiation of carbonaceous chondrites: A new view of space weathering on primitive asteroids, Icarus, 285, 43-57, doi:https://doi.org/10.1016/j.icarus.2016.12.019.

Lauretta, D. S., et al. (2019), The unexpected surface of asteroid (101955) Bennu, Nature, 568(7750), 55-60, doi:10.1038/s41586-019-1033-6.

Lauretta, D. S., X. Hua, and P. R. Buseck (2000), Mineralogy of fine-grained rims in the ALH81002 CM chondrite. , Geochim. Cosmochim. Acta 64, 3263–3273.

Le Corre, L., V. Reddy, J. A. Sanchez, D. Takir, E. Cloutis, A. Thirouin, K. J. Becker, J.-Y. Li, S. Sugita, and E. Tatsumi (2017), Ground-based characterization of Hayabusa2 mission target asteroid 162173 Ryugu: constraining mineralogical composition in preparation for spacecraft operations, Monthly Notices of the Royal Astronomical Society, 475(1), 614-623, doi:10.1093/mnras/stx3236.

MacKinnon, I. D. R. (1982), Ordered mixed-layer structures in the Mighei carbonaceous chondritic matrix. , Geochim. Cosmochim. Acta., 46, 479–489.

Malavergne, V., et al. (2014), How Mercury can be the most reduced terrestrial planet and still store iron in its mantle, Earth and Planetary Science Letters, 394, 186-197, doi:https://doi.org/10.1016/j.epsl.2014.03.028.

Matsuoka, M., T. Nakamura, T. Hiroi, K. Kitazato, M. A. T. Iwata, K. Amano, S. Kobayashi, T. Osawa, M. Ohtake, S. Matsuura, T. Arai, H. Senshu, M. Komatsu, A. Nakato, Y. Nakauchi, C. Pilorget, R. Brunetto, F. Poulet, L. Riu, D. Domingue, F. Vilas, D. Takir, E. Palomba, A., R. M. Galiano, D. Perna, A. Barucci, J-P Bibring, N. Imae, A. Yamaguchi, H. Kojima, S., and S. T. Nakazawa, M. Yoshikawa, S. Watanabe, Y. Tsuda (2019), Infrared Spectra of Asteroid Ryugu:

Comparison to Laboratory-Measured Carbonaceous Chondrites., 50th Lunar and Planetary Science Conference, Abstract #1534.

Maturilli, A., J. Helbert, M. D'Amore, I. Varatharajan, and Y. Rosas Ortiz (2018a), The Planetary Spectroscopy Laboratory (PSL): Wide spectral range, wider sample temperature range, in Infrared Remote Sensing and Instrumentation XXVI, edited, doi:10.1117/12.2319944.

Maturilli, A., J. Helbert, S. Ferrari, B. Davidsson, and M. D'Amore (2016), Characterization of asteroid analogues by means of emission and reflectance spectroscopy in the 1- to 100-µm spectral range, Earth, Planets and Space, 68(1), 113, doi:10.1186/s40623-016-0489-y.

Maturilli, A., J. Helbert, J. M. St. John, J. W. Head Iii, W. M. Vaughan, M. D'Amore, M. Gottschalk, and S. Ferrari (2014), Komatiites as Mercury surface analogues: Spectral measurements at PEL, Earth and Planetary Science Letters, 398, 58-65, doi:http://dx.doi.org/10.1016/j.epsl.2014.04.035.

Maturilli, A., J. Helbert, I. Varatharajan, Y Rosas Ortiz, and M. D'Amore (2018b), The Planetary Spectroscopy Laboratory (PSL), Earth and Planetary Science Congress (EPSC), Abstract: EPSC2018-753.

McAdam, M. M., J. M. Sunshine, K. T. Howard, and T. M. McCoy (2015), Aqueous alteration on asteroids: Linking the mineralogy and spectroscopy of CM and CI chondrites, Icarus, 245, 320-332, doi:https://doi.org/10.1016/j.icarus.2014.09.041.

Moskovitz, N. A., et al. (2013), Rotational characterization of Hayabusa II target Asteroid (162173) 1999 JU3, Icarus, 224(1), 24-31, doi:https://doi.org/10.1016/j.icarus.2013.02.009.

Nakamura, T. (2005), Post-hydration thermal metamorphism of carbonaceous chondrites, Journal of Mineralogical and Petrological Sciences, 100(6), 260-272, doi:10.2465/jmps.100.260.

Perna, D., et al. (2017), Spectral and rotational properties of near-Earth asteroid (162173) Ryugu, target of the Hayabusa2 sample return mission⋆, A&A, 599, L1.

Potin, S., P. Beck, L. Bonal, B. Schmitt, F. Moynier, E. Quirico, A. Garenne, and C. Honda (2018), Post-Accretion History and Reflectance Spectroscopy Properties of the Mukundpura Meteorite, 81st Annual Meeting of The Meteoritical Society 2018, LPI Contrib. No. 2067.

Potin, S., P. Beck, B. Schmitt, and F. Moynier (2019), Some things special about NEAs: Geometric and environmental effects on the optical signatures of hydration, Icarus, 333, 415-428, doi:https://doi.org/10.1016/j.icarus.2019.06.026.

Ray, D., and A. D. Shukla (2018), The Mukundpura meteorite, a new fall of CM chondrite, Planetary and Space Science, 151, 149-154, doi:https://doi.org/10.1016/j.pss.2017.11.005.

Reuter, D. C., et al. (2018), The OSIRIS-REx Visible and InfraRed Spectrometer (OVIRS): Spectral Maps of the Asteroid Bennu, Space Science Reviews, 214(2), 54, doi:10.1007/s11214-018-0482-9.

Richardson, S. M. (1981), Alteration of mesostasis in chondrules and aggregates from three C2 carbonaceous chondrites, Earth Planet. Sci. Lett., 52, 67-75.

Rudraswami, N. G., A. K. Naik, R. P. Tripathi, N. Bhandari, S. G. Karapurkar, M. S. Prasad, E. V. S. S. K. Babu, and U. V. R. Vijaya Sarathi (2018), Chemical, isotopic and amino acid composition of Mukundpura CM2.0 (CM1) chondrite: Evidence of parent body aqueous alteration, Geoscience Frontiers, doi:https://doi.org/10.1016/j.gsf.2018.02.001.

Ryskin, Y. I. (1974), The Vibrations of Protons in Minerals: hydroxyl, water and ammonium, The Infrared Spectra of Minerals, edited by V. C. Farmer, p. 0, Mineralogical Society of Great Britain and Ireland, doi:10.1180/mono-4.9.

Sasaki, S., S. Sugita, E. Tatsumi, C. H. H. Miyamoto, T. Morota, O. S. Barnouin, M. Hirabayashi, S. Kanda, M. Kanamaru, N. Hirata, T. Hiroi, T. Nakamura, T. Noguchi, R. Honda, T. Michikami, S. Watanabe, N. Namiki, P. Michel, S. Kameda,, and H. S. T. Kouyama, M. Yamada, H. Kikuchi, D. L. Domingue, Y. Cho, K. Yoshioka, M. Hayakawa, M. Matsuoka, R. Noguchi, N. Sakatani, H. Sawada, Y. Yokota, M. Yoshikawa (2019), Brightness and Morphology Variations on Surface Rocks of 162173 Ryugu: Space Weathering, Breccia Structure, and Meridional Cracks, 50th Lunar and Planetary Science Conference, Abstract: #1368.

Simon, A. A., D. C. Reuter, N. Gorius, A. Lunsford, R. G. Cosentino, G. Wind, D. S. Lauretta, and T. O.-R. Team (2018), In-Flight Calibration and Performance of the OSIRIS-REx Visible and IR Spectrometer (OVIRS), Remote Sensing, 10(9), 1486.

Sugita, S., et al. (2019), The geomorphology, color, and thermal properties of Ryugu: Implications for parent-body processes, Science, eaaw0422, doi:10.1126/science.aaw0422.

Takir, D., J. P. Emery, H. Y. Mcsween Jr., C. A. Hibbitts, R. N. Clark, N. Pearson, and A. Wang (2013), Nature and degree of aqueous alteration in CM and CI carbonaceous chondrites, Meteoritics & Planetary Science, 48(9), 1618-1637, doi:10.1111/maps.12171.

Tatsumi, E., S. Sugita, S. Kameda, R. Honda, T. Kouyama, Y. Yokota, N. Sakatani, T. M. C. Honda, M. Tomokatsu, M. Yamada, H., Y. C. Suzuki, M. Matsuoka, M. Hayakawa, K. Yoshioka, K. Ogawa, H. Sawada, F. Vilas, D., and L. L. C. Domingue, S. Sasaki, T. Nakamura, T. Hiroi (2019), Visible Color Variation of Boulders on 162173 Ryugu, 50th Lunar and Planetary Science Conference, Abstract: #1753.

Thompson, M. S., M. J. Loeffler, R. V. Morris, L. P. Keller, and R. Christoffersen (2019), Spectral and chemical effects of simulated space weathering of the Murchison CM2 carbonaceous chondrite, Icarus, 319, 499-511, doi:https://doi.org/10.1016/j.icarus.2018.09.022.

1138 Tomeoka, K., and P. R. Buseck (1985), Indicators of aqueous alteration in CM carbonaceous
1139 chondrites: Microtextures of a layered mineral containing Fe, S, O and Ni, Geochimica et
1140 Cosmochimica Acta, 49(10), 2149-2163, doi:https://doi.org/10.1016/0016-7037(85)90073-0.

1141 Vilas, F. (2008), Spectral Characteristics of Hayabusa2 Near-Earth Asteroid Targets 162173
1142 1999 JU3 and 2001 QC34, The Astronomical Journal, 135(4), 1101-1105, doi:10.1088/0004-
1143 6256/135/4/1101.

1144 Walsh, K. J., et al. (2019), Craters, boulders and regolith of (101955) Bennu indicative of an old
1145 and dynamic surface, Nature Geoscience, 12(4), 242-246, doi:10.1038/s41561-019-0326-6.

1146 Watanabe, S., et al. (2019), Hayabusa2 arrives at the carbonaceous asteroid 162173 Ryugu—A
1147 spinning top–shaped rubble pile, Science, eaav8032, doi:10.1126/science.aav8032.

1148 Zega, T. J., and P. R. Buseck (2003), Fine-grained-rim mineralogy of the Cold Bokkeveld CM
1149 chondrite, Geochim. Cosmochim. Acta, 67, 1711–1721.

1150 Zolensky, M. E., R. Barrett, and L. Browning (1993), Mineralogy and composition of matrix and
1151 chondrule rims in carbonaceous chondrites, Geochim. Cosmochim. Acta., 57, 3123–3148.